European Journal of Medicinal Chemistry 252 (2023) 115270

Contents lists available at ScienceDirect

European Journal of Medicinal Chemistry

journal homepage: www.elsevier.com/locate/ejmech

Research paper

Designed multiple ligands for the treatment of type 2 diabetes mellitus and its complications: Discovery of (5-arylidene-4-oxo-2-thioxothiazolidin-3-yl) alkanoic acids active as novel dual-targeted PTP1B/AKR1B1 inhibitors

Rosanna Maccari [a,*], Gerhard Wolber [b], Massimo Genovese [c], Gemma Sardelli [d], Valerij Talagayev [b], Francesco Balestri [d], Simone Luti [c], Alice Santi [c], Roberta Moschini [d], Antonella Del Corso [d], Paolo Paoli [c,**], Rosaria Ottanà [a]

[a] Department of Chemical, Biological, Pharmaceutical and Environmental Sciences, University of Messina, Viale F. Stagno d'Alcontres 31, 98166, Messina, Italy
[b] Molecular Design Lab, Institute of Pharmacy, Freie Universität Berlin, Königin-Luisestr. 2 + 4, 14195, Berlin, Germany
[c] Department of Scienze Biomediche Sperimentali e Cliniche, Sezione di Scienze Biochimiche, University of Firenze, Viale Morgagni 50, 50134, Firenze, Italy
[d] Department of Biology, Biochemistry Unit, University of Pisa, via S. Zeno, 51, 56123, Pisa, Italy

ARTICLE INFO

Keywords:
Diabetes mellitus
Multiple ligands
Protein tyrosine phosphatase 1B
Aldose reductase
4-thiazolidinone derivatives

ABSTRACT

Type 2 diabetes mellitus (T2DM) is a serious chronic disease with an alarmingly growing worldwide prevalence. Current treatment of T2DM mainly relies on drug combinations in order to control blood glucose levels and consequently prevent the onset of hyperglycaemia-related complications. The development of multiple-targeted drugs recently emerged as an attractive alternative to drug combinations for the treatment of complex diseases with multifactorial pathogenesis, such as T2DM. Protein tyrosine phosphatase 1B (PTP1B) and aldose reductase (AKR1B1) are two enzymes crucially involved in the development of T2DM and its chronic complications and, therefore, dual inhibitors targeted to both these enzymes could provide novel agents for the treatment of this complex pathological condition. In continuing our search for dual-targeted PTP1B/AKR1B1 inhibitors, we designed new (5-arylidene-4-oxo-2-thioxothiazolidin-3-yl)alkanoic acids. Among them, 3-(4-phenylbutoxy) benzylidene derivatives **6f** and **7f**, endowed with interesting inhibitory activity against both targets, proved to control specific cellular pathways implicated in the development of T2DM and related complications.

1. Introduction

Diabetes mellitus (DM) is a disease characterized by chronic hyperglycemia, which results from impaired insulin secretion by pancreatic β-cells or tissue insulin resistance. Currently, more than 530 million people worldwide suffer from DM and the number of cases is predicted to rise to almost 800 million by 2045; in addition, it is estimated that, only in the last year, more than 6 million deaths were attributable to DM. More than 90% of diabetic adults suffer from type 2 DM (T2DM), which is mainly characterized by insulin resistance, and the prevalence of this type of DM has alarmingly increased among young people [1,2].

Multiple hyperglycaemia-dependent dysfunctions cause tissue damage and are responsible for the development of serious chronic diabetic complications, particularly neuropathies, macroangiopathies and microangiopathies. Therefore, the therapeutic treatment of DM is fundamentally aimed to control hyperglycaemia. However, an adequate blood glucose control is difficult to achieve with a single drug, especially in advanced stages of the disease and, analogously to several other complex pathologies (such as cancer and neurodegenerative diseases), drug combinations are often required in order to achieve improved effectiveness.

Combination therapy can involve different issues, such as possible adverse drug-drug interactions and inappropriate pharmacokinetics. Therefore, as an alternative to drug combinations, a multi-target approach aimed to the identification of molecules simultaneously directed to selected multiple biomolecular targets (designed multiple ligands, DMLs) recently emerged as a promising strategy to develop new therapeutic agents for the treatment of multifactorial diseases [3–5]. This rational drug development process involves several challenges, one of which is the recognition of appropriate molecular targets, whose

* Corresponding author.
** Corresponding author.
E-mail addresses: rmaccari@unime.it (R. Maccari), paolo.paoli@unifi.it (P. Paoli).

https://doi.org/10.1016/j.ejmech.2023.115270
Received 30 January 2023; Received in revised form 8 March 2023; Accepted 8 March 2023
Available online 14 March 2023

implication in the pathogenetic mechanisms of the disease must be well-established. The structures of the different targets should also be well-characterized and share similar features in their binding sites. In addition, in the drug design pathway, after a first step aimed at identifying adequate DML scaffolds, an optimization process consists in balancing the multi-target activities and modulating drug-like properties of DMLs [3,5].

Among biomolecular targets critically implicated in the development of T2DM and its complications, protein tyrosine phosphatase 1B (PTP1B) and aldose reductase (AKR1B1) are two enzymes that play crucial roles.

PTP1B negatively regulates the insulin-signaling pathway through

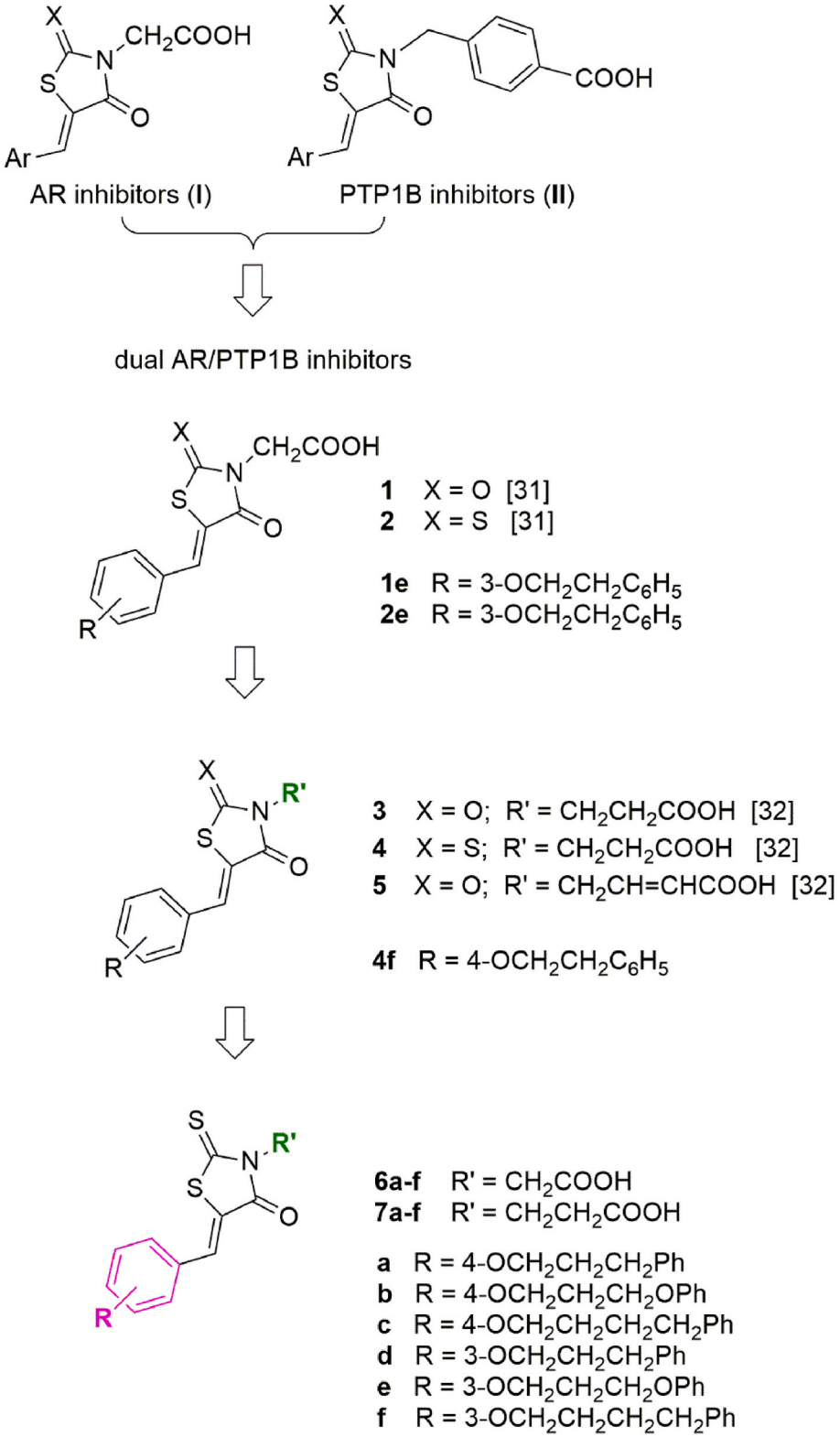

Fig. 1. Development of (5-arylidene-4-oxothiazolidin-3-yl)alkanoic acids as dual PTP1B/AKR1B1 inhibitors.

the dephosphorylation of specific residues of the activated insulin receptor (IR). It is well established that PTP1B dysregulation is critically involved in the development of insulin resistance, in both T2DM and some associated pathologies, such as obesity [6–8]. Accordingly, the inhibition of PTP1B can improve the cellular response to insulin, therefore making this enzyme an attractive target for developing new agents directed to the treatment of T2DM [9–11].

AKR1B1 is a member of the aldo-keto reductase superfamily, which is present in most human cells. It plays a determinant role in diabetic chronic complications, through the NADPH-dependent reduction of glucose to sorbitol, which in turn is oxidized to fructose by sorbitol dehydrogenase, in the polyol pathway. Under hyperglycaemic conditions, an increased flux of glucose through the polyol pathway occurs, which leads to osmotic imbalance, reduction of antioxidant cellular defense, promotion of protein glycation and inflammatory events, resulting in tissue damage that is responsible for the development of diabetic chronic complications [12,13]. AKR1B1 inhibitors were shown to prevent or control the progression of DM-associated pathologies, including neuropathy and retinopathy. Thus, AKR1B1 inhibitors represent promising agents for the treatment of hyperglycemia-induced pathologies associated with DM, as well as of other inflammatory diseases [14–16].

In this context, the design of novel inhibitors targeted to both PTP1B and AKR1B1 could allow the elicitation of favorable pharmacological effects and provide DMLs as novel agents for the treatment of T2DM and its complications.

A wide variety of promising selective inhibitors of AKR1B1 or PTP1B were reported so far [9,10,13,16–30], while the design of effective cell-permeable multiple inhibitors directed to both enzymes is still in its infancy. However, the knowledge acquired on the two individual targets and the structure-activity relationships (SARs) related to their inhibitors represent a feasible starting point for the design of dual PTP1B/AKR1B1 inhibitors.

Although PTP1B and AKR1B1 belong to different families of enzymes, some shared structural features can be exploited in order to design dual PTP1B/AKR1B1 inhibitors. In particular, previous studies which we carried out on 4-thiazolidinone derivatives as inhibitors of AKR1B1 or PTP1B (Fig. 1) showed that the pharmacophores of both classes of inhibitors include: a) a chain with an acidic tail on the N-3 of the thiazolidinone ring, and b) a lipophilic portion in position 5 of the heterocyclic scaffold, containing one or two aromatic portions [17–30].

According to a knowledge-based dual-targeting strategy, a first series of dual AKR1B1/PTP1B inhibitors was designed by merging the pharmacophores of (5-arylidene-4-oxothiazolidin-3-yl)acetic acid derivatives (**I**, Fig. 1), which exhibited excellent inhibitory activity towards AKR1B1 [17–24], and of 4-[(5-arylidene-4-oxothiazolidin-3-yl) methyl]benzoic acid derivatives (**II**, Fig. 1), which showed to be potent PTP1B inhibitors [25–30]. Among them, (2,4-dioxo-5-{[3-(2-phenylethoxy)phenyl]methylidene}thiazolidin-3-yl)acetic acid (**1e**) and the corresponding 2-thioxo-4-thiazolidinone **2e** (Fig. 1) attracted our interest because they showed to be potent AKR1B1 inhibitors (IC_{50} = 0.276 μM and 0.056 μM, respectively), also endowed with an appreciable ability to inhibit PTP1B at micromolar concentrations (IC_{50} = 32.5 μM and 12.4 μM, respectively) [31]. Studies of enzymatic kinetics and in silico molecular docking indicated that these compounds behave as reversible inhibitors of both human AKR1B1 and human PTP1B, with an uncompetitive and non-competitive mechanism of action toward AKR1B1 and PTP1B, respectively [31].

These findings paved the way for the design of inhibitors that can bind non-conserved regions of both PTP1B and AKR1B1, providing a promising tool for the discovery of new DMLs targeted to these enzymes. Therefore, in order to acquire further knowledge on the structural requirements necessary for the binding to these sites and the consequent simultaneous inhibition of both AKR1B1 and PTP1B, 3-(5-arylidene-4-oxothiazolidin-3-yl)propanoic acid derivatives **3**, **4** and 4-(5-arylidene-2,4-dioxothiazolidin-3-yl)-2-butenoic acid analogues **5** (Fig. 1) were designed and evaluated [32]. Out of them, 3-[4-oxo-{5-[4-(2-phenylethoxy)phenyl]methylidene}-2-thioxothiazolidin-3-yl]propanoic acid (**4f**, Fig. 1) stood out as a reversible inhibitor of both AKR1B1 and PTP1B, at low micromolar concentrations (IC_{50} AKR1B1 = 5.3 μM; IC_{50} PTP1B = 12.7 μM), also exhibiting insulin-sensitizing effects in C2C12 cell cultures [32]. Analogously to compounds **1e** and **2e**, selected compounds **3**, **4** behaved as uncompetitive AKR1B1 inhibitors and mixed or pure non-competitive PTP1B inhibitors. The relative SARs highlighted that the insertion of the propanoic acid residue on the thiazolidinone N-3 can increase the inhibitory potency towards PTP1B, although it reduces AKR1B1 inhibition compared with acetic acid derivatives, thus allowing dual PTP1B/AKR1B1 inhibitors to be obtained with a more balanced activity profile on the two target enzymes in comparison with previously reported compounds **1**, **2**. Moreover, the extension of the linker chain between the two benzene rings of the 5-arylidene portion proved to enhance especially the PTP1B inhibition, since this moiety appeared to be correlated to the potency against this enzyme with an activity order (2-phenylethoxy)benzylidene > benzyloxybenzylidene > phenoxybenzylidene. In addition, the presence of smaller and/or more polar substituents on the 5-benzylidene ring was unfavorable for PTP1B inhibition [31]. On the other hand, the inhibitory activity towards AKR1B1 showed to be less markedly influenced by the extension of the 5-arylidene portion, whereas the position of the substituent on the 5-benzylidene ring appeared to play an appreciable role [31,32].

Pursuing the objective to improve PTP1B inhibition levels, meanwhile maintaining good activity against AKR1B1, here we report the design and evaluation of a new series of [4-oxo-5-(phenyl/phenoxyalkoxy)benzylidene-2-thioxothiazolidin-3-yl]alkanoic acid derivatives (**6a-f** and **7a-f**, Fig. 1) bearing a further extension of the linker chain between the aromatic rings of the 5-arylidene portion. The newly-synthesized compounds **6** and **7** possess an acetic or propanoic chain on thiazolidinone N-3, which can be beneficial to achieve effective interactions with both target enzymes. Among compounds **6**,**7**, we identified new DMLs with interesting *in vitro/ex vivo* activities.

2. Results and discussion

2.1. Chemistry

2-(5-Arylidene-4-oxo-2-thioxothiazolidin-3-yl)acetic acids **6a-f** and 3-(5-arylidene-4-oxo-2-thioxothiazolidin-3-yl)propanoic acids **7a-f** were synthesized according to a procedure already reported [32], as depicted in Scheme 1.

Compounds **6**, **7** were obtained by Knoevenagel condensation between commercial (4-oxo-2-thioxothiazolidin-3-yl)acetic acid (**11**) or 3-(4-oxo-2-thioxothiazolidin-3-yl)propanoic acid (**12**) and the appropriate (phenyl/phenoxyalkoxy)benzaldehydes **10a-f** (Scheme 1). The reaction was carried out in refluxing glacial acetic acid, in the presence of sodium acetate. After cooling, crude solid was isolated and washed with water. Compounds **6a-f**, **7a-f** were obtained in good yields and ≥95% purity by recrystallization in methanol.

3-/4-(Phenyl/phenoxyalkoxy)benzaldehydes **10a-f** were synthesized by O-alkylation of the 3- hydroxybenzaldehyde (**8**) or 4-hydroxybenzaldehyde (**9**) with the suitable alkyl bromide, in anhydrous dimethylformamide, under stirring at 50 °C for about 8 h, using potassium carbonate as base (Scheme 1).

The structures of synthesized compounds **6a-f** and **7a-f** were assigned on the basis of analytical data and NMR spectroscopy (Supplementary Figs. S1-S24). All synthesized derivatives **6, 7** were obtained only as *Z* isomers, analogously to the previously reported 5-arylidene-4-thiazolidinones whose stereochemistry had been confirmed by X-ray crystallography [17,33]. In fact, all $^{1}H/^{13}C$ NMR spectra showed only one set of signals; in particular, ^{1}H NMR spectra showed only one singlet in the range 7.74–7.86 ppm attributable to the resonance of the 5-methylidene proton.

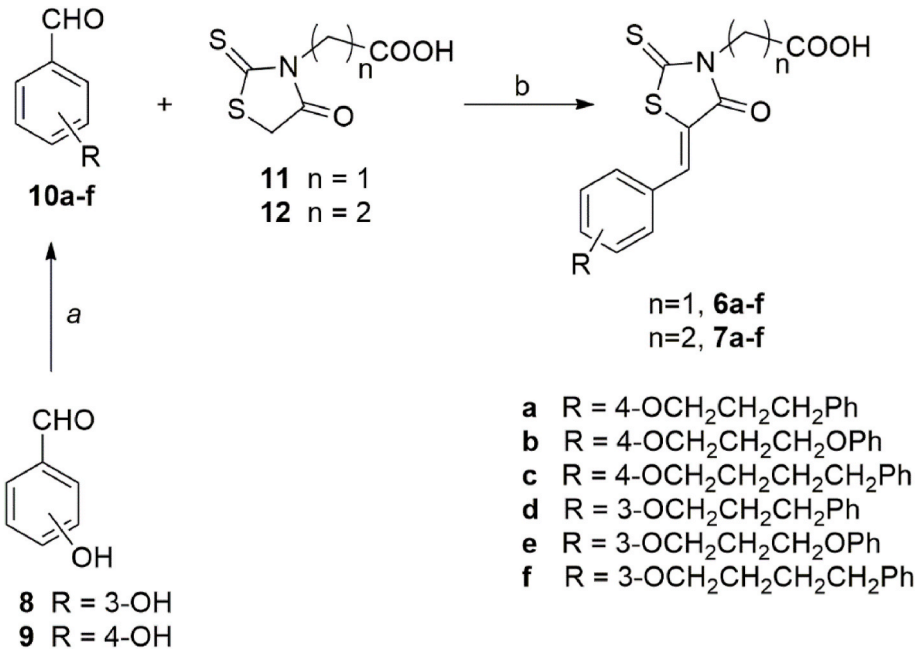

Scheme 1. Synthesis of 2-(5-arylidene-4-oxo-2-thioxothiazolidin-3-yl)acetic acids **6a-f** and 3-(5-arylidene-4-oxo-2-thioxothiazolidin-3-yl)propanoic acids **7a-f**.

In the ^{1}H NMR spectra of acetic acid derivatives **6**, the signal attributable to the protons of the methylene group on N-3 was present as a singlet at 4.66–4.74 ppm, while in the ^{13}C NMR spectra the corresponding carbon atom resonated at 45.6–46.2 ppm. In the ^{1}H NMR of propanoic acid derivatives **7**, the propanoic chain on N-3 gave rise to two triplets at 2.62–2.64 ppm and 4.12–4.23 ppm.

Furthermore, in ^{13}C NMR spectra of all synthesized compounds **6**, **7**, the 4-oxo-2-thioxothiazolidin-3-yl system gave rise to some diagnostic singlets originating from the resonance of the thiocarbonyl group in position 2 (at 193.6–193.8 ppm) as well as from the carbonyl in position 4 (in the range 166.8–167.3 ppm) and the carboxylic group of the chain on the N-3 (in the range 167.8–172.3 ppm).

2.2. *In vitro* enzyme inhibition

The *in vitro* inhibitory ability of compounds **6a-f**, **7a-f** was evaluated against both human recombinant PTP1B, by using *p*-nitrophenylphosphate as substrate and sodium metavanadate as reference drug, and human recombinant AKR1B1, by using L-idose as substrate and epalrestat as reference drug (Table 1).

All tested compounds **6a-f** and **7a-f** proved to be generally potent inhibitors of human AKR1B1, with IC_{50} values in a range from low-micromolar to nanomolar concentrations; in particular, compounds **6d**, **6e** and **6f** proved to be more active than Epalrestat, which is the only AKR1B1 inhibitor approved as drug in some Asian countries, so far [13]. Compounds **6d**, **6e** and **6f** were considered as tight binding inhibitors, since they showed IC_{50} values of the same order of magnitude of the enzyme concentration in the assay (i.e. 67 nM, see Methods). By comparing the AKR1B1 inhibitory potency of compounds **6a-f** and **7a-f**, it emerged that (5-arylidene-4-oxo-2-thioxothiazolidin-3-yl)acetic acids **6** are better inhibitors (from 18- to 184-fold) than propionic acid analogues **7**, in agreement with SARs previously acquired for analogous carboxylic acids [32]. Moreover, among acetic acids **6**, the *meta*-substituted derivatives (**6d-f**) appeared to be from 3- to 5-fold better inhibitors of AKR1B1 than *para*-substituted analogues (**6a-c**); however, the influence of the 5-arylidene moiety on the AKR1B1 inhibitory ability appeared to be moderate, since the IC_{50} values of compounds **6** are within a narrow range (from 0.05 μM to 0.33 μM). On the other hand, among propanoic acid derivatives **7a-f**, significant differences in

Table 1
Inhibitory activities of compounds **6a-f** and **7a-f** against human AKR1B1, PTP1B and TC-PTP.

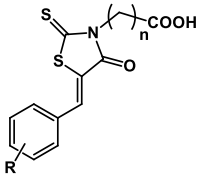

Compd	n	R	AKR1B1 IC_{50} (μM)[a]	PTP1B IC_{50} (μM)[a]	TC-PTP IC_{50} (μM)[a]
6a	1	4-$OCH_2CH_2CH_2Ph$	0.26 ± 0.06	79.0 %[b]	n.d.
6b	1	4-$OCH_2CH_2CH_2OPh$	0.22 ± 0.04	87.6 %[b]	n.d.
6c	1	4-$OCH_2CH_2CH_2CH_2Ph$	0.33 ± 0.04	4.0 ± 0.2	192.7 ± 49.5
6d	1	3-$OCH_2CH_2CH_2Ph$	0.05 ± 0.01	81.0 %[b]	n.d.
6e	1	3-$OCH_2CH_2CH_2OPh$	0.08 ± 0.01	100 %[b]	n.d.
6f	1	3-$OCH_2CH_2CH_2CH_2Ph$	0.06 ± 0.003	4.3 ± 0.5	9.0 ± 0.33
7a	2	4-$OCH_2CH_2CH_2Ph$	38.2 ± 3.8	99.8 %[b]	n.d.
7b	2	4-$OCH_2CH_2CH_2OPh$	3.9 ± 0.4	74.4 %[b]	n.d.
7c	2	4-$OCH_2CH_2CH_2CH_2Ph$	60.7 ± 11.7	2.9 ± 0.6	9.1 ± 0.22
7d	2	3-$OCH_2CH_2CH_2Ph$	1.2 ± 0.1	67.6 %[b]	n.d.
7e	2	3-$OCH_2CH_2CH_2OPh$	2.1 ± 0.6	77.0 %[b]	n.d.
7f	2	3-$OCH_2CH_2CH_2CH_2Ph$	2.1 ± 0.2	3.2 ± 0.2	25.8 ± 0.7
Epalrestat			0.10 ± 0.005		
Vanadate				0.4 ± 0.01	

[a] Values reported in the table represent the IC_{50} ± SE.
[b] Residual activity of PTP1B determined in the presence of the tested compound (5 μM). n.d.: not determined.

AKR1B1 inhibition ability were observed varying the 5-arylidene portion (IC_{50} values ranging from 1.2 μM to 60.7 μM); once again, the *meta*-substituted derivatives **7d-f** turned out to be better inhibitors than the *para*-substituted counterparts **7a-c** (Table 1).

It is worth pointing out that among propanoic acid derivatives **7**, 4-(3-phenoxypropoxy)benzylidene derivative **7b** proved to be 15-fold more active than 4-(4-phenylbutoxy)benzylidene analogue **7c**, suggesting that in this case the oxygen atom of the distal phenoxy group in the arylidene moiety could establish additional bonds with AKR1B1. On the contrary, the activity of the other phenoxyalkoxy derivatives (**6b, 6e, 7e**) was similar to that of the 4-phenylbutoxy isosteres (**6c, 6f, 7f**).

Regarding PTP1B, compounds **6c**, **6f**, **7c**, and **7f**, which bear a 4-phenylbutoxy group on the 5-benzylidene ring, were found to be the most potent PTP1B inhibitors, with very similar IC_{50} values ranging between 2.9 μM and 4.3 μM (Table 1), regardless of the *para* or *meta* position of the 4-phenylbutoxy group as well as of the presence of an acetic or propanoic chain on N-3. All other analogues **6a**, **6b**, **6d**, **6e** and **7a**, **7b**, **7d**, **7e** showed negligible activity, being scarcely active or completely inactive at 5 μM concentration (Table 1). These findings indicated that the 4-phenylbutoxy moiety could play a crucial role in the interaction with the target enzyme and, accordingly, limited modifications of the linker chain, such as the replacement of the distal methylene group with an oxygen atom (compounds **6b, 6e, 7b, 7e**) or its removal (compounds **6a, 6d, 7a, 7d**) caused a dramatic reduction of the PTP1B inhibitory effectiveness.

In order to evaluate the specificity of PTP1B inhibitors **6c**, **6f**, **7c** and **7f**, IC_{50} values toward TC-PTP were determined (Table 1 and Supplementary Fig. S25). This PTP shares a high sequence similarity with PTP1B [34] and, for this reason, it is often used to evaluate the degree of specificity of PTP1B inhibitors. Data obtained indicated that the selected compounds inhibit PTP1B more effectively than TC-PTP (Table 1). Their specificity toward PTP1B over TC-PTP decreased as follows: **6c** > **7f** > **7c** > **6f**. Interestingly, acetic acid derivative **6c** and propanoic acid derivative **7f** exhibited significant selectivity, with IC_{50} values toward TC-PTP which were 48-fold and 8-fold higher than those determined for PTP1B, respectively. However, in contrast with PTP1B inhibition, clear relationships between the substituent in the position 3 and 5 of the thiazolidinone core and TC-PTP inhibition did not emerge. In fact, the TC-PTP inhibition data of acetic derivatives **6c** and **6f** indicated that the 4-phenylbutoxy moiety was detrimental for the inhibition of this enzyme when inserted in the *para* position of the 5-benzyliene ring; on the contrary, the *para*-substituted propanoic acid derivative **7c** was more active as TC-PTP inhibitor than its *meta*-substituted counterpart **7f** (Table 1).

Overall, the *in vitro* evaluation of PTP1B/AKR1B1 inhibitory effects of alkanoic acids **6** and **7** allowed three promising dual inhibitors to be identified, i.e. compounds **6c, 6f** and **7f**, which exhibited interesting activity toward both target enzymes at low micromolar or nanomolar concentrations. Out of them, propanoic acid derivative **7f** stood out as a DML endowed with balanced effectiveness against both PTP1B (IC_{50} = 3.2 μM) and AKR1B1 (IC_{50} = 2.1 μM), whereas the corresponding acetic acid analogue **6f** proved to be the DML with the highest potency against AKR1B1 (IC_{50} = 0.06 μM) accompanied by a good PTP1B inhibition (IC_{50} = 4.3 μM). On the basis of these results, alkanoic acids **6c, 6f** and **7f** were selected for further investigation, by kinetic analyses and *ex vivo* assays.

It is worth noting that calculated physicochemical and pharmacokinetic parameters of compounds **6c, 6f** and **7f** indicated promising drug-likeness and predicted good oral bioavailability for these molecules, without Lipinski's rule violations (Supplementary Table S1).

2.3. Kinetics analyses

Based on the data above, additional studies were carried out to define the mechanism of action of selected compounds **6c**, **6f**, and **7f**, as dual PTP1B/AKR1B1 inhibitors, and of **7c**, as the most potent PTP1B inhibitor. Firstly, we evaluated whether these compounds behave as reversible or irreversible inhibitors. Using the dilution assay method, compounds **6c**, **6f**, **7c**, and **7f** were shown to act as reversible inhibitors of PTP1B (Supplementary Fig. S26). In the case of AKR1B1, **6c**, **6f**, and **7f** also resulted reversible inhibitors; in fact it was possible to observe an almost complete (>90%) recovery of the enzyme activity after removal of the inhibitors upon extensive dialysis.

Then, we evaluated the impact of increasing inhibitor concentrations on main kinetic parameters (K_M and V_{max}) of PTP1B (Fig. 2 and Supplementary Figs. S27–S30). The obtained results indicated that **6c** and **6f** behave as non-competitive inhibitors of PTP1B, while **7c** and **7f** act as mixed-type non-competitive inhibitors. The values of K_i and K_i', calculated using the appropriate equations, are reported in Table 2.

Primary data obtained in the kinetic characterization of **6c**, **6f** and **7f** as AKR1B1 inhibitors are reported in supplementary materials (Supplementary Figs. S31 and S32). Secondary plots used for the determination of inhibition constants K_i and K'_i are reported in Figs. 3–5 for compounds **6c**, **6f** and **7f**, respectively. It turned out that the three selected inhibitors act as mixed non-competitive inhibitors of AKR1B1. However, as reported in Table 2, in all cases K'_i values resulted lower (from twice to 4-fold) in comparison with K_i values, suggesting for these compounds a preferential interaction with the ES complex rather than with the free enzyme. In the case of **6f**, due to its feature of tight binding inhibitor, the inhibition constants were derived using Morrison equation (see Methods).

2.4. PTP1B and AKR1B1 docking experiments

PTP1B kinetic studies showed that **6c** and **6f** act as pure non-competitive inhibitors, whereas **7c** and **7f** displayed mixed-type non-competitive inhibition. Therefore, docking studies into both the catalytic binding site and the previously described allosteric binding site of PTP1B [31,32] were performed.

The obtained docking poses of **6c, 6f, 7c** and **7f** into the previously described allosteric binding site of PTP1B [31,32] (Fig. 6) showed comparable lipophilic contacts of the terminal phenyl ring with residues Arg79, Pro206 and Pro210. Docking poses of **6c, 6f** and **7c** display ionic interactions of carboxylic groups with residues Lys103, Arg 105 and Arg169. The orientation of the 2-thioxothiazolidin-4-one moiety of **7c** was different from the one observed in **7f**, thus preventing the propionic acid moiety from forming hydrogen bonding interactions with Lys103 and Arg169, displayed in the docking pose of **7f**, and only showing a hydrogen bonding interaction of the propionic moiety with Arg105.

Docking studies of **6c, 6f, 7c** and **7f** in the catalytic site of PTP1B (Fig. 7) displayed hydrogen bonding of acetic and propionic acid moieties with the side chain of Arg 221 and the backbones of Phe182 and Ser216. The terminal phenyl ring of **6c, 6f, 7c** and **7f** exhibits equivalent lipophilic contacts with residues Arg24, Ala27 and Met258 in the non-catalytic aryl phosphatase binding site. Lipophilic contacts of the butoxyphenyl substituent in position 3 of the 5-benzylidene ring of **6f** and **7f** with Tyr46 and Val49 were observed in the docking studies, which were comparable to the lipophilic contacts of the butoxyphenyl substituent in position 4 of the 5-benzylidene of **6c** and **7c** with the above-named residues. The propionic moiety allows **7c** and **7f** to progress further into the catalytic binding pocket, which reduces the hydrogen bonding interaction distance of the propionic moiety with the previously mentioned residues Phe182, Ser216 and Arg221 and minimizes the distance between the propionic moiety and key residue Phe182, thus favouring a crucial lipophilic contact. This lipophilic interaction was not observed in the docking poses of **6c** and **6f**, which act as pure non-competitive PTP1B inhibitors and showcases the importance of the propionic moiety in the mixed-type inhibition of **7c** and **7f**.

The difference in the surface shape of the polar head of **6c** and **7c** (Fig. 8) proved that the propionic acid moiety is beneficial for the affinity in the catalytic binding site of PTP1B, since a smaller distance to

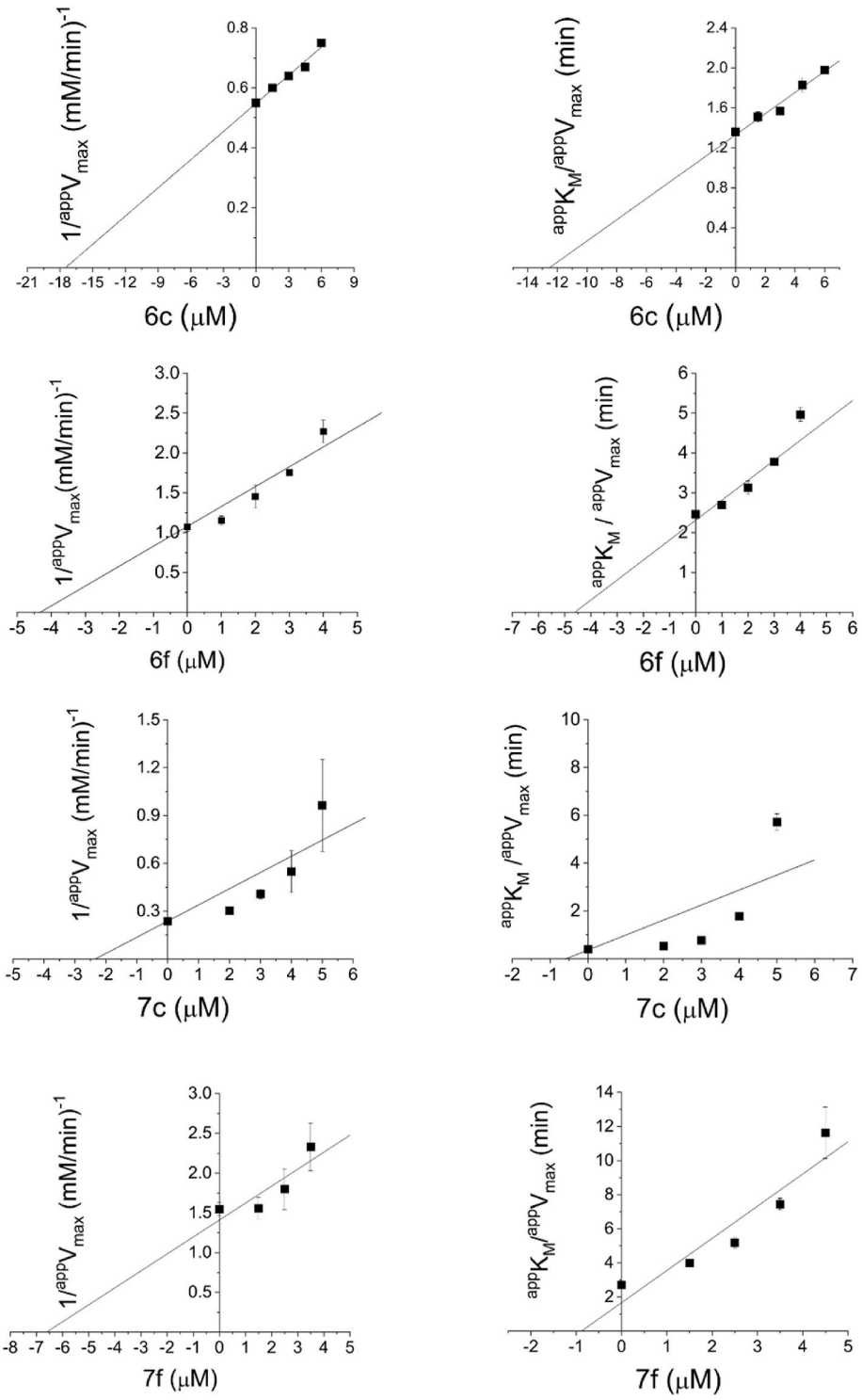

Fig. 2. Kinetic characterization of compounds **6c, 6f, 7c** and **7f** as PTP1B inhibitors.

Phe182 was observed for the propionic moiety of **7c** compared to the acetic moiety of **6c**. The docking studies were in accordance with the kinetic studies and allowed to further describe the different inhibitory potency between **6c, 6f, 7c** and **7f**.

In order to rationalize the preeminent influence that the alkanoic chain on thiazolidinone N-3 proved to exert on AKR1B1 inhibitory activity, docking experiments were carried out with the best dual inhibitors **6f** and **7f**. In particular, considering that, as described above, kinetic studies indicated a preferential interaction of these inhibitors with the AKR1B1/substrate (L-idose) complex rather than with the free enzyme, docking simulations were performed with the AKR1B1-idose complex. The obtained docking poses of **6f** and **7f** within the AKR1B1-idose complex (Fig. 9) showed consistent ionic and hydrogen bonding interactions with residues Arg217 and Lys221. The thioxothiazolidinone moiety of **6f** and **7f** displays a hydrogen bond with the backbone of Ala299. The acetic moiety of **6f** enables the 5-benzylidene ring to showcase lipophilic contacts with residues Trp219 and Leu302, whereas the propionic moiety of **7f** leads to a rotation of the 5-benzylidene ring, which is more exposed to solvent and a further distance from residue Leu302 compared to **6f**, thus displaying only a lipophilic contact with

Table 2
Inhibition constants of compounds **6c**, **6f**, **7c** and **7f** for PTP1B and AKR1B1.[a]

Inhibitor	PTP1B		AKR1B1	
	K_i (μM)	K'_i (μM)	K_i (μM)	K'_i (μM)
6c	12.1 ± 0.5	17.5 ± 2.4	1.3 ± 0.3	0.41 ± 0.02
6f	4.6 ± 0.9	4.3 ± 0.5	0.08 ± 0.01	0.03 ± 0.01
7c	0.6 ± 0.2	2.4 ± 0.4	n.d.	n.d.
7f	0.9 ± 0.1	6.6 ± 3.5	4.0 ± 0.1	1.1 ± 0.1

n.d.: not determined.
[a] K_i and K'_i refer to the apparent dissociation constants for the EI and ESI complex, respectively.

residue Trp219. The different conformation of the 5-benzylidene ring enables **6f** to advance further into the binding pocket, thus allowing **6f** to establish a lipophilic contact with residue Trp20 in addition to lipophilic interactions to residues Val49 and Phe122, present in both **6f** and **7f** docking poses.

2.5. Ex Vivo assays

2.5.1. Effects of selected compounds 6c, 6f, 7c, and 7f on insulin signaling pathway and cellular glucose uptake

The effects of selected compounds **6c**, **6f**, **7c**, and **7f** on insulin signaling pathway were evaluated on murine C2C12 cell line. The cytotoxicity of the selected compounds was assessed by measuring the viability of differentiated C2C12 cells incubated for 24 h with each compound (20 μM final concentration). The results are showed in Fig. 10. Interestingly, we observed that none of compounds caused a significant reduction of cell viability at 20 μM concentration.

Subsequently, differentiated C2C12 cells were starved for 24 h and then incubated at 37 °C for 15 min with insulin (10 nM) or with

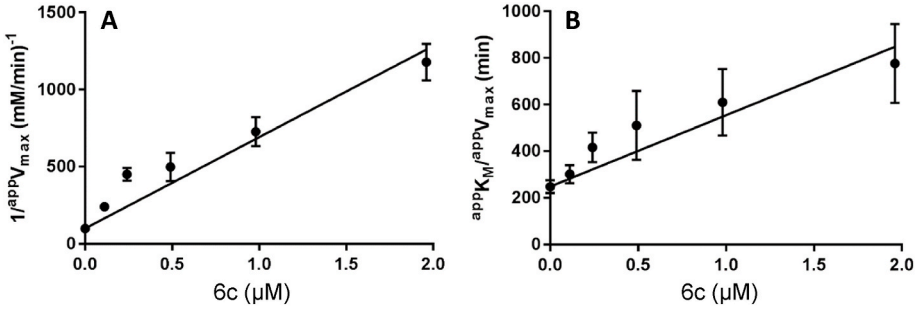

Fig. 3. Kinetic characterization of compound **6c** as AKR1B1 inhibitor. The secondary plots of $1/^{app}V_{max}$ (Panel A) and $^{app}K_M/^{app}V_{max}$ (Panel B) derived from primary plot (see Supplementary Fig. S31), as a function of the inhibitor concentration, are reported. Error bars (when not visible are within the symbol size) represent the standard deviations of the mean from at least three independent experiments.

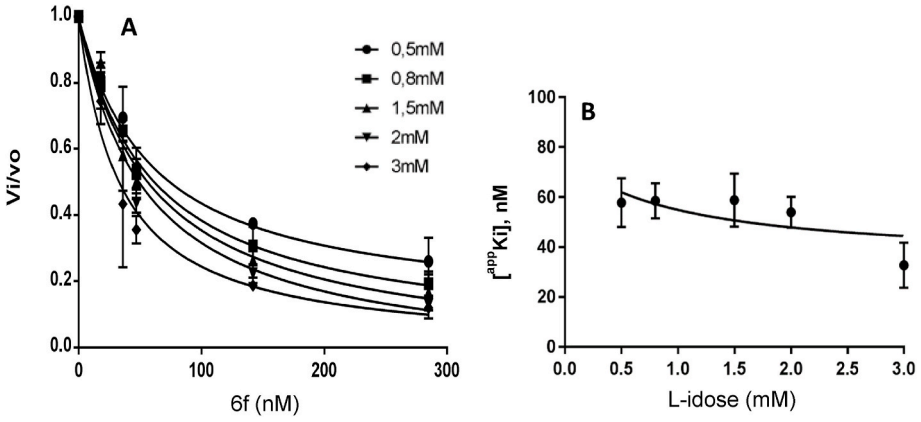

Fig. 4. Kinetic characterization of compound **6f** as AKR1B1 inhibitor. Panel A: the activity of the purified AKR1B1 (8 mU) was measured at the indicated concentrations of the inhibitor in the presence of the indicated L-idose concentrations. Curves were plotted by non-linear regression analysis fitting the experimental data to Morrison equation (see Methods). Error bars (when not visible are within the symbol size) represent the standard deviations of the mean from at least three independent experiments. Panel B: the apparent inhibition constant ($^{app}K_i$) values determined from Panel A for each substrate concentration were plotted against substrate concentration and fitted by non-linear regression analysis to equation (1) (see Methods), relative to a general case of tight binding non-competitive inhibition model, for the evaluation of inhibition constants.

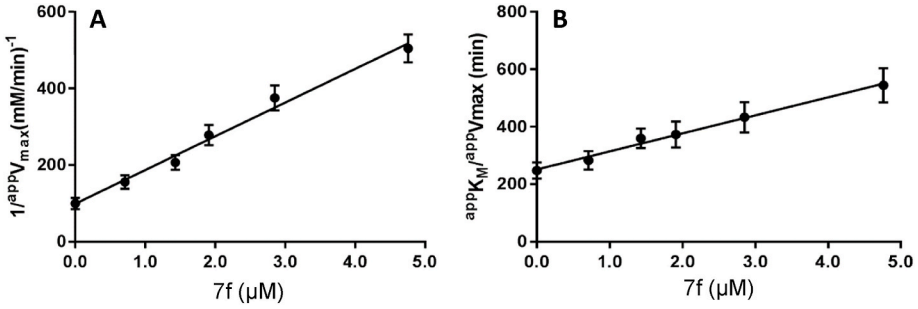

Fig. 5. Kinetic characterization of compound **7f** as AKR1B1 inhibitor. The secondary plots of $1/^{app}V_{max}$ (Panel A) and $^{app}K_M/^{app}V_{max}$ (Panel B) derived from primary plot (see Supplementary Fig. S32), as a function of the inhibitor concentration, are reported. Error bars (when not visible are within the symbol size) represent the standard deviations of the mean from at least three independent experiments.

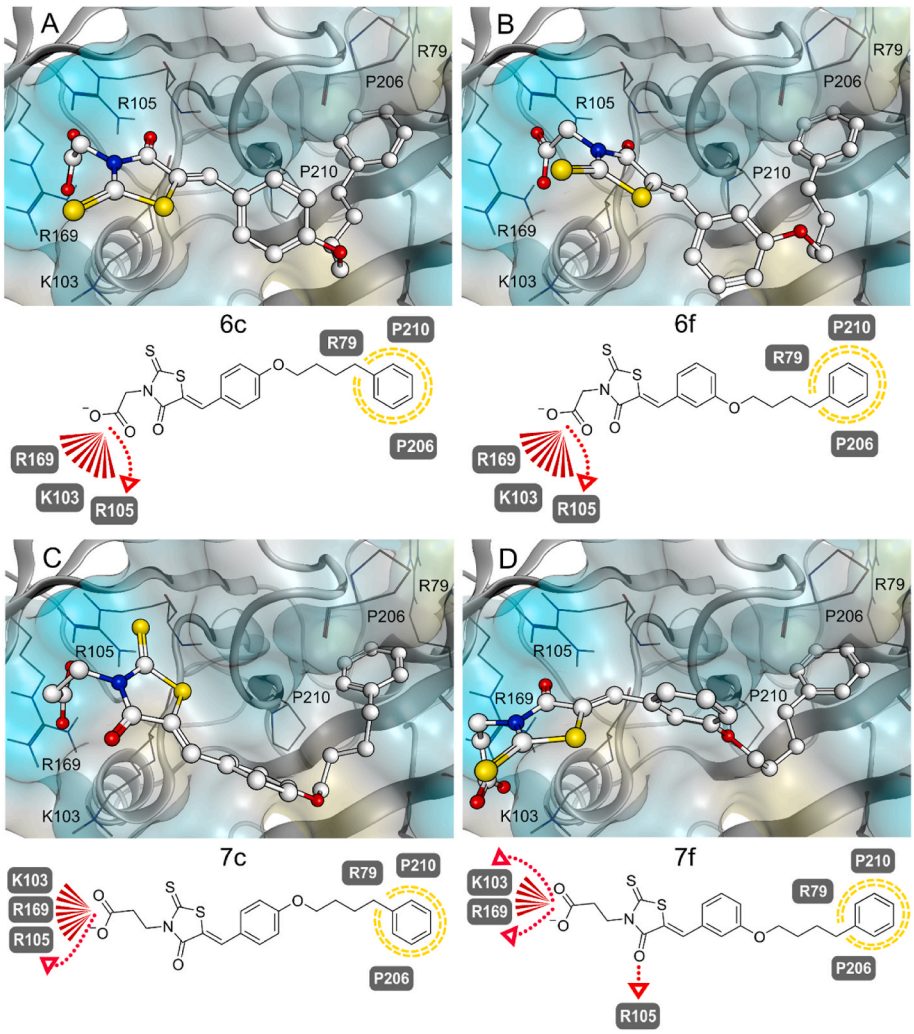

Fig. 6. 3D and 2D depictions of **6c, 6f, 7c** and **7f** in the PTP1B allosteric binding site. (A) 3D and 2D depiction of selected **6c** pose. (B) 3D and 2D depiction of selected **6f** pose. (C) 3D and 2D depiction of selected **7c** pose. The rotation of thioxothiazolidinone is less favorable and prevents **7c** from forming hydrogen bonding interactions with residues Lys103 and Arg169. (D) 3D and 2D depiction of selected **7f** pose. The rotation of thioxothiazolidinone is more favorable and allows **7f** to move further into the binding pocket and establish a hydrogen bonding interaction with residues Lys103, Arg105 and Arg169. Blue surface visualizes hydrophilic regions and yellow surface lipophilic regions. Yellow dotted lines indicate lipophilic contacts, red arrows hydrogen bonding interactions and red lines anionic interactions.

compounds **6c, 6f, 7c**, **7f** both alone and in combination with insulin. After this time, cells were washed and lysed to evaluate phosphorylation levels of kinase Akt. Western blots are shown in Fig. 11.

Western blot analysis (Fig. 11) revealed that the treatment with **6f**, **7c** and, at a lesser extent, **7f** alone enhanced the phosphorylation levels of kinase Akt, while compound **6c** resulted completely ineffective. Interestingly, the highest values of pAkt/Akt ratio were observed for cells treated with insulin-compound combinations, suggesting that **6f, 7c**, and **7f** could act as potent insulin-sensitizing agents.

Although compounds **7c** and **7f** showed comparable activity against PTP1B, the former resulted to be the least active inhibitor of AKR1B1. Therefore, we carried out further assays on compounds **6f** and **7f**, which resulted to be potent inhibitors of both targets.

To better evaluate the impact of compounds on insulin signalling pathway, the ability of **6f** and **7f** to stimulate cellular glucose uptake was also investigated. Myoblasts C2C12 were starved for 24 h and then stimulated with 10 nM insulin or 20 μM compounds **6f** and **7f** for 15 min. Then, the medium was removed, cells were washed with PBS and then incubated for 3 h at 37 °C with starvation medium containing 40 μM 2-NBDG. The amount of fluorescent glucose incorporated into myoblasts was quantified analysing cells by using a flow cytometer. Data obtained are reported in Fig. 12.

The results of the glucose incorporation assay showed that levels of fluorescent glucose incorporated into the cells treated with **6f, 7f**, and the combinations of insulin plus compound were very similar one each other. These data indicated that compounds **6f** and **7f** alone act as potent insulin-mimetic agent and that combined treatments did not increase the amount of incorporated glucose in comparison to single compound treatments. All together, these data suggested that compounds **6f** and **7f** behave as insulin-mimetic compounds more than insulin-sensibilizing agents.

Although Western blot analyses showed that the treatment with combinations insulin plus **6f** or **7f** strongly increased Akt phosphorylation, glucose incorporation tests showed that the treatment with the compounds alone was as effective as the combined treatment. We hypothesized that these differences were mainly due to the low levels of Akt expression detected by the Western blot after co-stimulation with insulin plus **6f** or **7f**. Based on the experimental data, we speculated that a lower Akt level could be the result of an increase in the degradation rate or, alternatively, due to the inability of antibodies used to recognize their target. To assess whether co-stimulation resulted in increased protein degradation, we analysed the total protein content of the samples using the SDS-PAGE method. After staining the gel with colloidal Coomassie, we observed that neither treatment with compounds **6f** or **7f** alone nor treatment with insulin plus compounds caused a decrease in the overall cellular protein content (Fig. 13). Therefore, we concluded that low detection levels of Akt after co-stimulation could result from the inability of antibodies to recognize this target after combined treatment rather than from increased protein degradation.

Indeed, the antibodies used to assess total Akt levels bind to the carboxy terminal sequence of Akt, a domain that has several other phosphorylation sites, besides Ser473. Based on this evidence, we

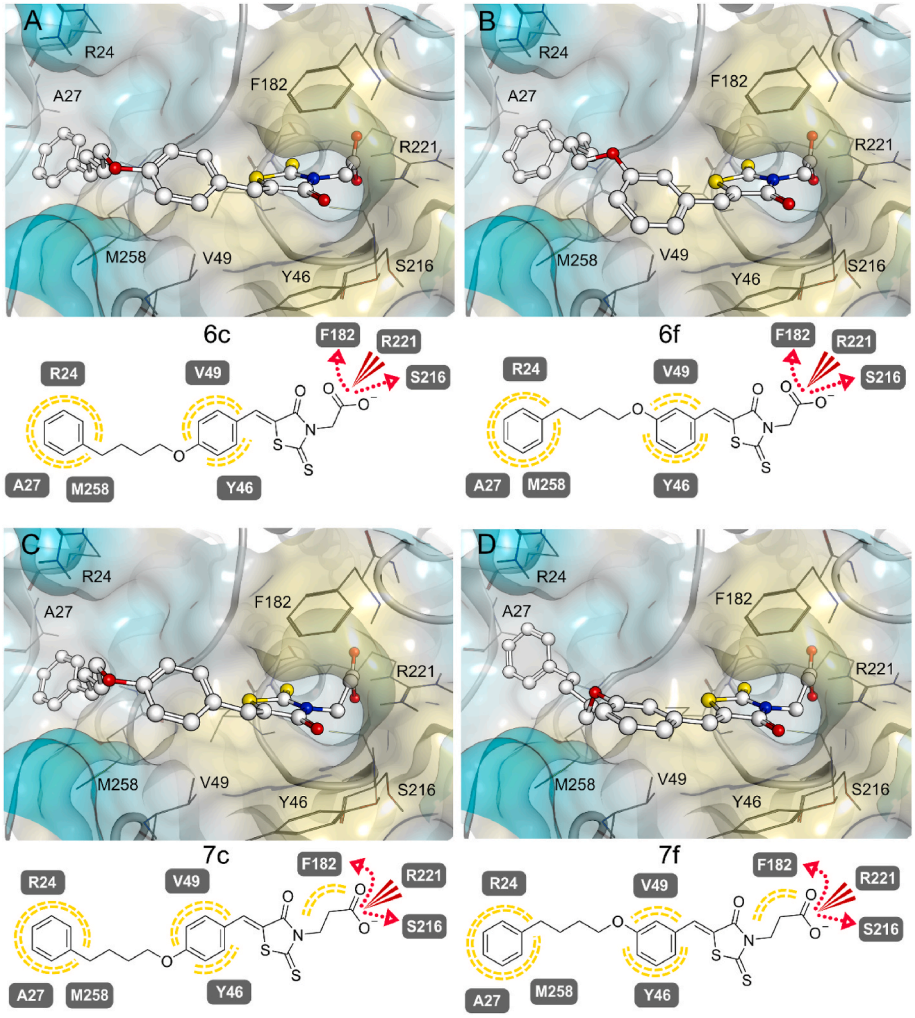

Fig. 7. 3D and 2D depictions of **6c, 6f, 7c** and **7f** in the PTP1B catalytic binding site. (A) 3D and 2D depiction of selected **6c** pose. (B) 3D and 2D depiction of selected **6f** pose. (C) 3D and 2D depiction of selected **7c** pose. (D) 3D and 2D depiction of selected **7f** pose. The propionic moiety of **7c** and **7f** permits the ligand to advance further into the catalytic binding pocket and obtain a crucial lipophilic contact with residue Phe182. Yellow dotted lines indicate lipophilic contacts, red arrows hydrogen bonding interactions and red lines anionic interactions.

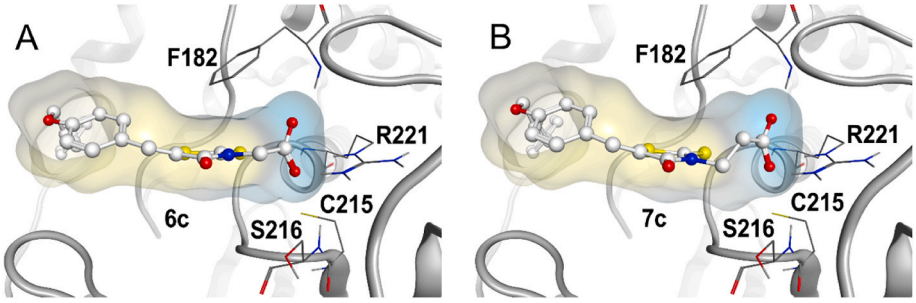

Fig. 8. Ligand surface shapes of **6c** and **7c** in the PTP1B catalytic binding site. (A) Binding site of **6c** displays a more distanced ligand surface from Phe182 and no lipophilic contact can be observed. (B) Binding site of **7c** showcases a complementary ligand surface and displays a lipophilic contact with Phe182.

speculated that the ability of **6f** and **7f** to inhibit PTP1B could strongly stimulate insulin pathway, resulting in an enhanced phosphorylation of residues located in carboxy-terminal region of Akt, thereby impairing the recognition by antibodies raised against the unphosphorylated form of this protein.

Our results demonstrated that compounds **6f** and **7f** possess strong insulin-mimetic activity rather than insulin-sensitizing activity. This finding might seem contrary to the concept that an inhibitor capable of targeting PTP1B, an enzyme that acts as a negative regulator of the activated form of the IR, should enhance insulin activity, and not act as an insulin-mimetic agent by itself.

However, the insulin-mimetic activity of PTP1B inhibitors could be explained by considering the peculiar structure of the IR. In fact, unlike most hormone or growth factor receptors, the IR is naturally dimeric and possesses a low intrinsic tyrosine kinase activity, even in the absence of insulin [35]. Based on this evidence, it is reasonable to think that under starvation, the activity of PTP1B is necessary to dampen the spontaneous phosphorylation of the IR, thus contributing to its complete inactivation. According to this hypothesis, the exposure of the glucose transporter GLUT4 on the cell membrane is decreased in adipocytes that overexpress PTP1B, both during fasting and after a meal [36]. Taken together, these findings suggest that PTP1B damps basal phosphorylation levels of IR during fasting and that the inhibition of PTP1B activity could be expected to increase the basal level of IR phosphorylation, leading to the

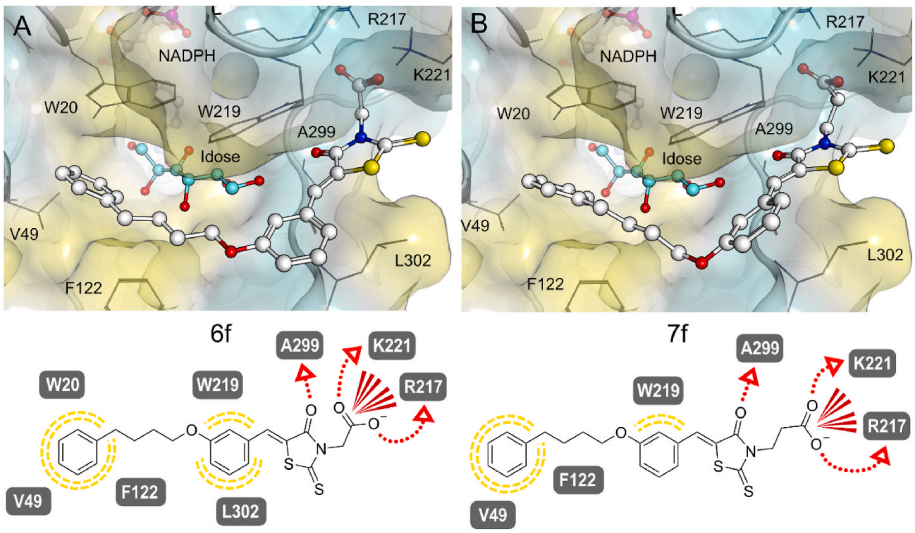

Fig. 9. 3D and 2D depictions of **6f** and **7f** within the AKR1B1-idose complex. (A) 3D and 2D depiction of the selected **6f** pose. (B) 3D and 2D depiction of the selected **7f** pose. The rotation of the 5-benzylidene ring of **6f** reduces the distance to residue Leu302 and allows the ligand to advance further into the binding pocket, granting two additional lipophilic contacts. Yellow dotted lines indicate lipophilic contacts, red arrows hydrogen bonding interactions and red lines anionic interactions.

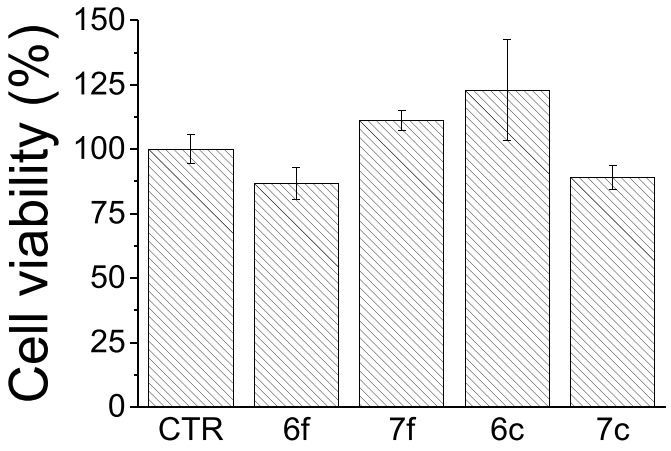

Fig. 10. Cell viability assay. Differentiated C2C12 cells were incubated in the presence of 20 μM of each compound for 24 h in complete medium. After this time, medium was withdrawn and cells washed with PBS. Then, cells were incubated for 60 min with 500 μL of complete medium containing 0.5 mg/mL of MTT salt. After 30 min, cells were recovered, washed with PBS, and the lysed with 400 μL of DMSO to ensure cell lysis and the solubilization of formazane crystals present inside the cells. The absorbance of each sample was determined measuring the absorbance of samples using a microplate reader. Each test was carried out in quadruplicate. Data reported in the figure represent the mean value ± SD (n = 4). Data were normalized respect to control samples that consist in differentiated C2C12 cells incubated with the same volume of DMSO, the solvent used to solubilize each compound.

activation of insulin signaling.

In the past, several examples of small molecule PTP1B inhibitors showing *in vivo* insulin-mimetic activity were described. Bleasdale et al. showed that some cholecystokinin (CCK)-derived peptidomimetic compounds act as potent and specific PTP1B inhibitors and promote IR activation. Indeed, they observed that in rat skeletal (L6) myoblast cells, one of these compounds increased the magnitude of tyrosine phosphorylation of IR and the rate of absorption of 2-[^{3}H]deoxyglucose even in the absence of insulin, thus behaving as an insulin-mimetic compound [37]. In 2003, Xie et al. studied the effect of new small molecule PTP1B inhibitors on insulin signalling pathway in different insulin-sensitive cell lines. They observed that the most potent molecules acted as both insulin-mimetics and sensitizers, thereby validating the notion that small molecule PTP1B inhibitors could be used as antidiabetic drugs [38]. In 2004, Wiesmann et al. reported that some benzbromarone derivatives behaved as potent and specific allosteric PTP1B inhibitors and were able to enhance insulin signalling in chinese hamster ovary cells. Interestingly, the authors of this study demonstrated that such compounds not only acted as insulin sensitizing agents, but were also able to activate the insulin signalling pathway also in the absence of insulin co-stimulation, thus acting as insulin-mimetic agents [39]. Therefore, it is evident that the ability to act as insulin-mimetic compounds is not a peculiarity of compounds **6f** and **7f** but rather a common property shared by other PTP1B inhibitors.

2.5.2. *Effects of compound **6f** on intracellular sorbitol content*

Taking into account the results obtained from *in vitro* inhibition assays, compound **6f** proved to be the PTP1B/AKR1B1 dual inhibitor endowed with the most potent activity against AKR1B1. Therefore, we evaluated the ability of compound **6f** to interfere with sorbitol accumulation in a cell model of hyperglycemia, using cultured human lens epithelial line B3 (HLE) cells. The incubation of HLE cells in the presence of **6f** at 2 μM concentration did not significantly affect cell viability (Fig. 14). As expected, the exposure of HLE cells to high glucose concentrations (i.e. 75 mM D-glucose for 24 h) determined a twofold increase of intracellular sorbitol content (Fig. 15). A significant impairment of sorbitol accumulation was observed when glucose treatment was performed in the presence of **6f** at 2 μM concentration, whereas the reference drug sorbinil caused a similar reduction of sorbitol accumulation at higher concentration (10 μM) (Fig. 15).

3. Conclusions

As part of our search for DMLs as potential agents for the treatment of T2DM and related complications, the design and evaluation of (5-arylidene-4-oxo-2-thioxothiazolidin-3-yl)alkanoic acids **6a-f** and **7a-f** led to the identification of new derivatives endowed with noticeable dual PTP1B/AKR1B1 inhibitory activity. Propanoic acid derivative **7f** exhibited the most balanced dual-targeted profile, since it proved to inhibit both human PTP1B and AKR1B1 at similar low micromolar concentrations. The promising activity of compound **7f** resulted from the combination of the insertion of the propanoic acid residue on thiazolidinone N-3 along with the elongation of the linker chain between the two aromatic rings of the 5-arylidene moiety. The SAR investigation revealed that the features of the moieties inserted in the positions 3 and

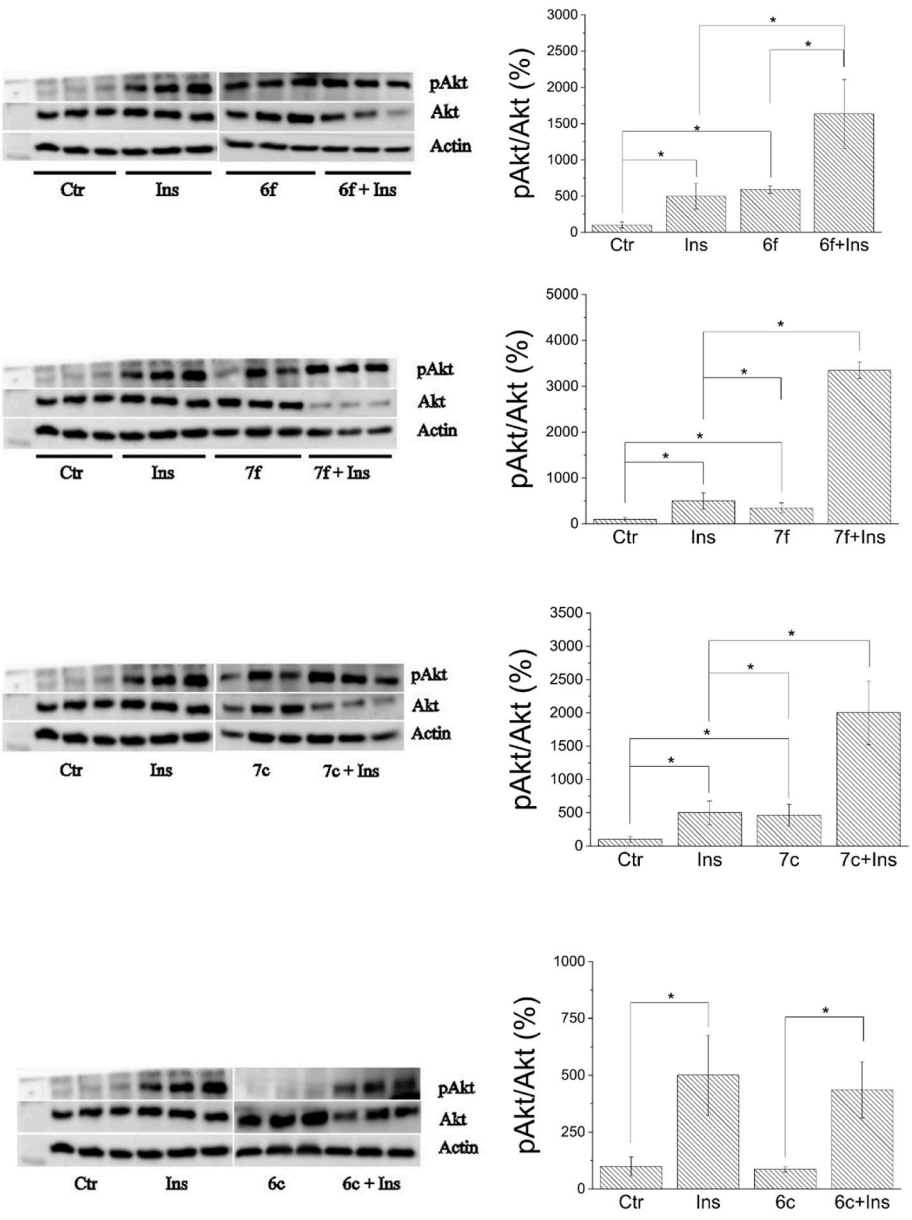

Fig. 11. Effect of **6c, 6f, 7c** and **7f** on insulin signaling pathway. C2C12 cells were starved and then stimulated for 15 min with 10 nM insulin, 20 μM of each compound or insulin-compound combination. After 15 min, cells were washed with cold PBS and lysed using 1X Laemmli sample buffer solution. *On the left*: proteins of the extracts were separated by SDS-PAGE and transferred on a PVDF membrane by western blotting. Phosphorylation status and total expression levels of kinase Akt were determined using specific antibodies for phosphorylated and unphosphorylated form of Akt. Levels of actin were detected to evaluate the amount of samples loaded on gel. Each test were carried out in triplicate. *On the right*: quantification of the intensity of Western blot bands. Data reported in the figure represent the mean value ± SD (n = 3). *p < 0.05.

5 of the thiazolidinone scaffold can significantly influence the inhibitory activities toward both PTP1B and AKR1B1, thus allowing the effectiveness profile towards these target enzymes to be modulated. Molecular docking experiments provided data congruent with the observed SARs, suggesting a crucial involvement of these portions in the interaction with catalytic and non-catalytic sites of both PTP1B and AKR1B1.

Interestingly, (4-phenylbutoxy)benzylidene derivatives **6f** and **7f** showed PTP1B inhibitory potency similar to that of previously investigated benzoic acid analogues **II** (Fig. 1) which, however, had proven to be inactive against AKR1B1. Therefore, the replacement of the *p*-methylbenzoic acid residue of compounds **II** with an alkanoic (acetic or propanoic) chain proved to be a favorable structural modification to obtain DMLs capable to inhibit both PTP1B and AKR1B1.

The evaluation of compounds **6f** and **7f** in cell systems suggested that they can behave as insulin-mimetic agents, since they remarkably improved glucose uptake in murine C2C12 myoblasts both in the presence and absence of insulin, through the activation of insulin signalling. In addition, compound **6f**, which showed higher potency against AKR1B1 than **7f**, significantly reduced the AKR1B1-dependent sorbitol accumulation into human lens epithelial line B3 cells, thus proving to be able to control a determinant event responsible for the onset of diabetic complications.

On the whole, the findings here reported provided another piece of knowledge which can encourage further development of cell-permeable DMLs able to control signalling pathways correlated with both PTP1B and AKR1B1, which are crucially involved in the pathogenesis of T2DM and associated complications.

4. Experimental section

4.1. Chemistry

Melting points were recorded on a Kofler hot-stage apparatus and are uncorrected. TLC controls were carried out on precoated silica gel plates (F 254 Merck). Rf values were determined by using appropriate mixtures of diethyl ether/*n*-hexane as eluent. Combustion analyses (C, H, N), determined by means of a C. Erba mod. 1106 elem. Analyzer, were within ±0.4% of the theoretical values. ^{1}H and ^{13}C NMR spectra were recorded on a Varian 500 MHz spectrometer operating at 499.74 and 125.73 MHz, respectively. Chemical shifts δ are given in ppm and

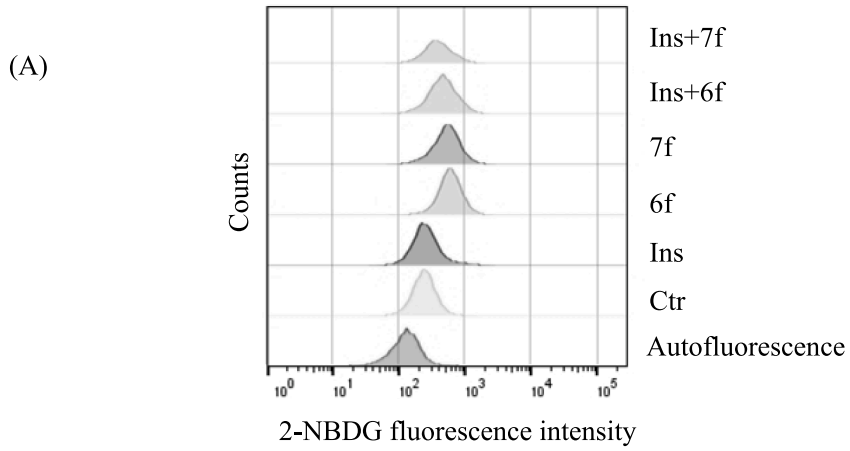

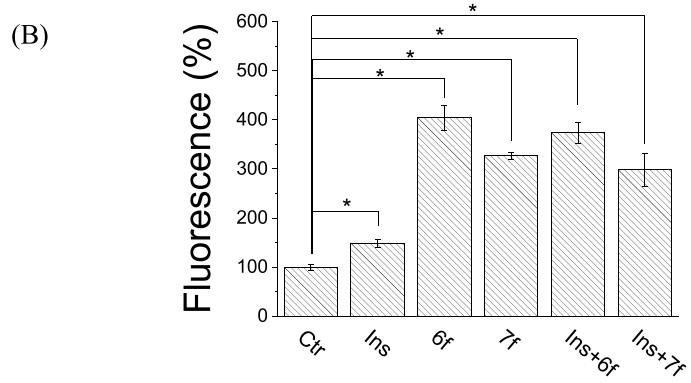

Fig. 12. Glucose uptake assay. C2C12 myoblasts were starved for 24 h and then stimulated with 10 nM insulin, 20 μM **6f** and **7f**, or with Ins-**6f**, Ins-**7f** combination for 15 min. After, the starvation medium was removed and cells were washed with PBS before to add starvation medium containing 40 μM of 2-NBDG. After 3 h, medium was removed, cells washed with PBS and trypsinized. Cells were collected and analysed using a FACS Canto II flow cytometer (BD Bioscence). (A) Representative flow plots of 2-NBDG uptake in C2C12 myoblasts obtained using FlowJo software. (B) Quantitative analysis of obtained data. All tests were carried out in quadruplicate. Data reported represent the mean fluorescence value ± SD. *$p < 0.05$, **$p < 0.01$.

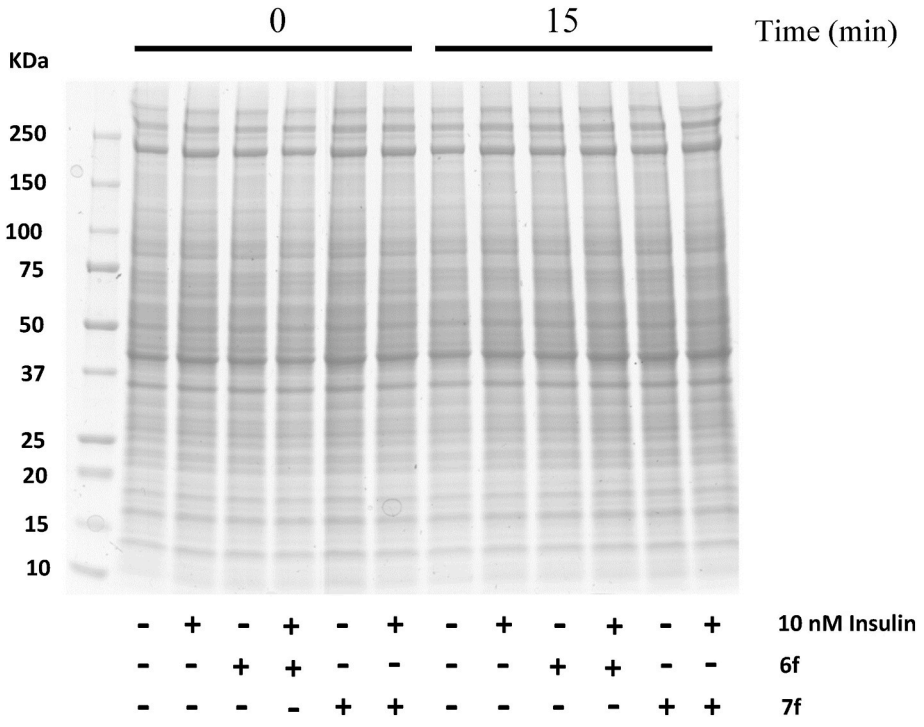

Fig. 13. SDS-PAGE of protein extracts. Myotubes were starved and then stimulated with 10 nM insulin, 20 μM **6f** and **7f** alone and in combination with insulin for 15 min. After stimulation, cells were lysed using 1X Laemmli sample buffer solution. Then, protein extracts were collected, transferred in Eppendorf tubes and boiled for 5 min. The same volumes of protein samples (10 μL) were loaded in each lane. After the run, cellular proteins were highlighted by staining the gel with colloidal Coomassie.

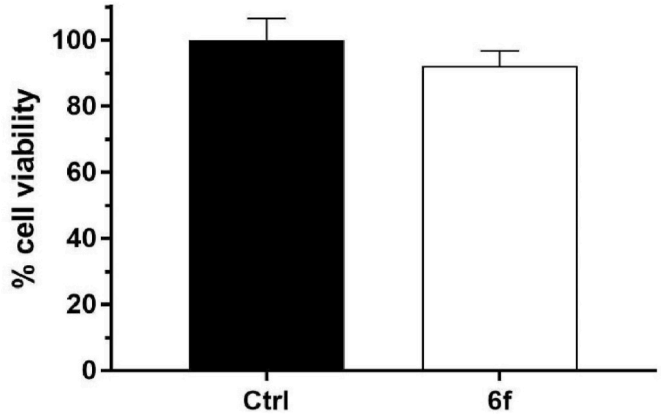

Fig. 14. Effect of **6f** on cell viability. HLE cells were cultured as described in the Methods section. Cell viability was measured in presence of 0.05% DMSO both in the absence (Ctrl) and in the presence of **6f** at the final concentration of 2 μM. The reported values are the mean ± SEM of eleven independent measurements. Statistical analysis was performed using Student's T test. Significance was evaluated with respect to untreated cells (p value = 0.34).

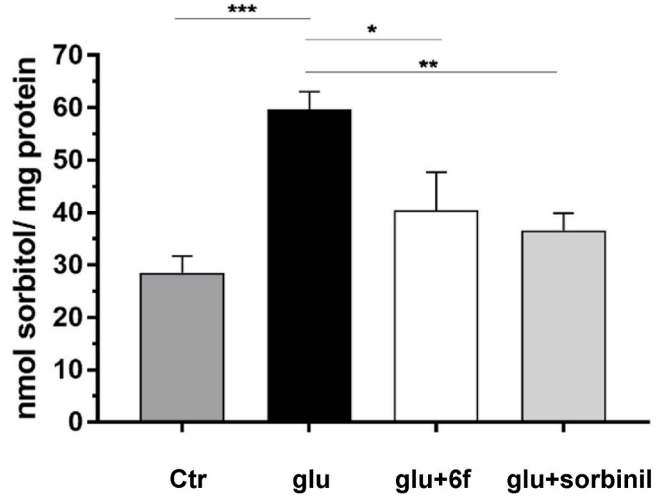

Fig. 15. Effect of **6f** on sorbitol accumulation. HLE cells were incubated for 24 h in the indicated conditions and sorbitol content was measured (see Methods) and reported as nmol of sorbitol/mg of protein. Bars refer to: *Ctr*: control; *glu*: 75 mM D-glucose; *glu*+***6f***: 75 mM D-glucose +2 μM **6f**; *glu* + *sorbinil*: 75 mM D-glucose +10 μM sorbinil. The reported values are the mean ± SEM of six independent measurements. Statistical analysis was performed using one way ANOVA with Tukey post hoc test. Significance was evaluated as indicated (*p < 0.1; **p < 0.01; ***p < 0.001).

coupling constants are expressed in Hz. All the spectra were phased, baseline was corrected where necessary and $CDCl_3$ or DMSO-d_6 signals were used as a reference for both ^1H and ^{13}C spectra. All exchangeable protons were confirmed by addition of D_2O. Unless stated otherwise, all materials were obtained from commercial suppliers and used without further purification.

The purity of synthetic compounds was established as ≥ 95% by combustion analysis.

*4.1.1. General procedure for the synthesis of (phenyl/phenoxyalkoxy) benzaldehydes **10a-f***

To a mixture of 3-/4-hydroxybenzaldehyde (2 g, 16.4 mmol), and potassium carbonate (9.06 g, 65.6 mmol) in anhydrous DMF (75 mL) the appropriate alkyl bromide (26.6 mmol) was added in small portions at regular intervals of few minutes; the mixture was stirred at 40–50 °C for 2–4 h. Then water (20 ml) was added and the mixture was acidified until pH 5–6 and extracted with ethyl acetate. The organic layer was washed with H_2O (10 × 100 ml), dried with anhydrous Na_2SO_4 and the solvent was removed under reduced pressure. The crude mixture was chromatographed on a silica gel column (eluant petroleum ether: diethyl ether = 9 : 1 or cyclohexane:diethyl ether = 8:2) to provide pure aldehydes ***10a-f***.

*4.1.1.1. 4-(3-Phenylpropoxy)benzaldehyde **10a**.* Yield 85%; yellow oil; ^1H NMR ($CDCl_3$): δ 2.14–2.22 (m, 2H, CH_2); 2.85 (t J = 7.65 Hz, 2H, $CH_2C_6H_5$); 4.06 (t J = 6.30 Hz, 2H, OCH_2); 7.01 (m, 2H, arom); 7.22–7.24 (m, 3H, arom); 7.31–7.34 (m, 2H, arom); 7.85 (m, 2H, arom); 9.90 (s, 1H, CHO). ^{13}C NMR ($CDCl_3$): δ 30.8, 32.0, 68.1 (CH_2); 115.2, 125.9, 128.5, 128.7, 128.9, 131.7, 141.9, 165.4 (CH arom, Cq arom); 190.5 (C═O).

*4.1.1.2. 4-(3-Phenoxypropoxy)benzaldehyde **10b**.* Yield 95%; yellow oil; ^1H NMR ($CDCl_3$): δ 2.31 (m, 2H, CH_2); 4.18 (t J = 6.0 Hz, 2H, $CH_2OC_6H_5$); 4.27 (t J = 6.15 Hz, 2H, OCH_2); 6.93 (d J = 8.75 Hz, 1H, arom); 6.97 (t J = 7.4 Hz, 1H, arom); 7.03 (m, 2H, arom); 7.30 (dd J = 8.75 Hz e J = 7.4 Hz, 1H, arom); 7.84 (m, 2H, arom); 9.89 (s, 1H, CHO). ^{13}C NMR ($CDCl_3$): δ 30.0, 65.0, 65.1 (CH_2); 115.0, 119.9, 128.1, 128.9, 132.1, 159.2, 165.0 (CH arom, Cq arom); 191.1 (C═O).

*4.1.1.3. 4-(4-Phenylbutoxy)benzaldehyde **10c**.* Yield 89%; yellow oil; ^1H NMR ($CDCl_3$): δ 1.83–1.86 (m, 4H, 2 CH_2); 2.71 (t J = 7.05 Hz, 2H, $CH_2C_6H_5$); 4.05 (t J = 6.15 Hz, 2H, OCH_2); 6.98 (m, 2H, arom); 7.20–7.22 (m, 3H, arom); 7.28–7.30 (m, 2H, arom); 7.82 (m, 2H, arom); 9.88 (s, 1H, CHO). ^{13}C NMR ($CDCl_3$): δ 29.0, 29.2, 35.4, 68.8 (CH_2); 114.8, 128.3, 128.6, 128.9, 140.0, 142.1, 165.1 (CH arom, Cq arom); 191.0 (C═O).

*4.1.1.4. 3-(3-Phenylpropoxy)benzaldehyde **10d**.* Yield 73%; yellow oil; ^1H NMR ($CDCl_3$): δ 2.19 (m, 2H, CH_2); 2.87 (t J = 7.35 Hz, 2H, $CH_2C_6H_5$); 4.05 (t J = 6.30 Hz, 2H, OCH_2); 7.20–7.27 (m, 3H, arom); 7.33–7.36 (m, 3H, arom); 7.42–7.50 (m, 3H, arom); 9.99 (s, 1H, CHO). ^{13}C NMR ($CDCl_3$): δ 30.9, 32.2, 68.2 (CH_2); 116.1, 120.4, 121,6, 126.0, 128.3, 128.7, 129.6, 137.7, 142.2, 165.3 (CH arom, Cq arom); 191.1 (C═O).

*4.1.1.5. 3-(3-Phenoxypropoxy)benzaldehyde **10e**.* Yield 77%; yellow oil; ^1H NMR ($CDCl_3$): δ 2.31 (m, 2H, CH_2); 4.18 (t J = 6.05 Hz, 2H, $CH_2OC_6H_5$); 4.25 (t J = 6.15 Hz, 2H, OCH_2); 6.92–6.97 (m, 2H, arom); 7.18–7.21 (m, 1H, arom); 7.28–7.31 (m, 2H, arom); 7.42–7.47 (m, 3H, arom); 9.98 (s, 1H, CHO). ^{13}C NMR ($CDCl_3$): δ 30.1, 64.9, 65.0 (CH_2); 114.5, 115.8, 120.1, 120.3, 121.7, 129.1, 129.9, 137.1, 159.3, 165.2 (CH arom, Cq arom); 191.2 (C═O).

*4.1.1.6. 3-(4-Phenylbutoxy)benzaldehyde **10f**.* Yield 75%; yellow oil; ^1H NMR ($CDCl_3$): δ 1.87–1.91 (m, 4H, 2 CH_2); 2.75 (t J = 7.20 Hz, 2H, $CH_2C_6H_5$); 4.06 (t J = 6.05 Hz, 2H, OCH_2); 7.19–7.27 (m, 3H, arom); 7.34–7.37 (m, 3H, arom); 7.43–7.49 (m, 3H, arom); 10.0 (s, 1H, CHO). ^{13}C NMR ($CDCl_3$): δ 29.1, 29.2, 36.0, 68.9 (CH_2); 116.1, 120.3, 121.7, 126.1, 128.3, 128.5, 129.9, 138.0, 143.0, 165.1 (CH arom, Cq arom); 191.1 (C═O).

*4.1.2. General procedure for the synthesis of (5-arylidene-4-oxo-2-thioxothiazolidin-3-yl)acetic acids **6a-f***

A mixture of (4-oxo-2-thioxothiazolidin-3-yl)acetic acid (0.40 g, 2.09 mmol), glacial acetic acid (10 mL), sodium acetate (2.13 g, 15.7 mmol) and the appropriate aldehyde **10** (0.50 g, 2.09 mmol) was refluxed for 3–4 h. The mixture was cooled and poured into H_2O, providing a precipitate which was filtered off, washed with H_2O and recrystallized from methanol to give pure (5-arylidene-4-oxo-2-thioxothiazolidin-3-yl) acedic acids **6a-f**.

4.1.2.1. 2-{(5Z)-4-oxo-5-[4-(3-phenylpropoxyphenyl)methylidene]-2-thioxothiazolidin-3-yl}acetic acid ***6a.*** Yield 30%; yellow solid; m.p. 218–220 °C; ^{1}H NMR (DMSO-$d_{6\delta}$): δ 2.04 (m, 2H, CH_2); 2.75 (t J = 7.45 Hz, 2H, C$H_2C_6H_5$); 4.06 (t J = 6.35 Hz, 2H, OCH_2); 4.74 (s, 2H, NCH_2); 7.12 (m, 2H, arom); 7.18 (m, 1H, arom); 7.22–7.24 (m, 2H, arom); 7.27–7.30 (m, 2H, arom); 7.63 (m, 2H, arom); 7.85 (s, 1H, CH methylidene); 13.44 (br s, 1H, COOH). ^{13}C NMR (DMSO-$d_{6\delta}$): δ 30.7, 32.0, 45.6, 67.8 (CH_2); 116.2, 119.0, 125.9, 126.5, 128.9, 129.0, 133.7, 134.7, 141.8, 161.7 (C-5, CH methylidene, CH arom, Cq arom); 167.0 (C═O); 167.9 (COOH); 193.7 (C═S). Anal. ($C_{21}H_{19}NO_4S_2$) calcd: C 61.00; H 4.63; N 3.39; found: C 60.98; H 4.24; N 3.45.

4.1.2.2. 2-{(5Z)-4-oxo-5-[4-(3-phenoxypropoxyphenyl)methylidene]-2-thioxothiazolidin-3-yl}acetic acid ***6b.*** Yield 54%; yellow solid; m.p. 181–182 °C; ^{1}H NMR (DMSO-$d_{6\delta}$): δ 2.19 (m, 2H, CH_2); 4.12 (t J = 6.15 Hz, 2H, $CH_2OC_6H_5$); 4.23 (t J = 6.20 Hz, 2H, OCH_2); 4.73 (s, 2H, NCH_2); 6.91–6.95 (m, 3H, arom); 7.13 (m, 2H, arom); 7.27 (t J = 7.45 Hz, 2H, arom); 7.61 (m, 2H, arom); 7.82 (s, 1H, CH methylidene); 13.49 (br s, 1H, COOH). ^{13}C NMR (DMSO-$d_{6\delta}$): δ 29.1, 45.6, 64.5, 65.4 (CH_2); 114.9, 116.2, 119.0, 121.1, 126.0, 130.0, 133.7, 134.7, 159.0, 161.6 (C-5, CH methylidene, CH arom, Cq arom); 167.0 (C═O); 167.9 (COOH); 193.6 (C═S). Anal. ($C_{21}H_{19}NO_5S_2$) calcd: C 58.73; H 4.46; N 3.26; found: C 58.84; H 4.27; N 3.44.

4.1.2.3. 2-{(5Z)-4-oxo-5-[4-(4-phenylbutoxyphenyl)methylidene]-2-thioxothiazolidin-3-yl}acetic acid ***6c.*** Yield 45%; yellow solid; m.p. 198–200 °C; ^{1}H NMR (DMSO-$d_{6\delta}$): δ 1.73 (m, 4H, 2 CH_2); 2.64 (t J = 7.0 Hz, 2H, C$H_2C_6H_5$); 4.08 (t J = 6.0 Hz, 2H, OCH_2); 4.66 (s, 2H, NCH_2); 7.10 (m, 2H, arom); 7.17 (m, 1H, arom); 7.20–7.22 (m, 2H, arom); 7.26–7.29 (m, 2H, arom), 7.61 (m, 2H, arom); 7.82 (s, 1H, CH methylidene). ^{13}C NMR (DMSO-$d_{6\delta}$): δ 27.9, 28.7, 35.3, 46.2, 68.4 (CH_2); 116.2, 119.2, 125.9, 128.7, 129.0, 133.6, 134.3, 134.4, 142.5, 161.7 (C-5, CH methylidene, CH arom, Cq arom); 167.1 (C═O); 167.8 (COOH); 193.6 (C═S). Anal. ($C_{22}H_{21}NO_4S_2$) calcd: C 61.81; H 4.95; N 3.28; found: C 61.54; H 4.75; N 3.10.

4.1.2.4. 2-{(5Z)-4-oxo-5-[3-(3-phenylpropoxyphenyl)methylidene]-2-thioxothiazolidin-3-yl}acetic acid ***6d.*** Yield 69%; yellow solid; m.p. 142–144 °C; ^{1}H NMR (DMSO-$d_{6\delta}$): δ 2.04 (m, 2H, CH_2); 2.75 (t J = 7.5 Hz, 2H, $CH_2C_6H_5$); 4.02 (t J = 6.35 Hz, 2H, OCH_2); 4.74 (s, 2H, NCH_2); 7.09 (d J = 8.3 Hz, 1H, arom); 7.17–7.24 (m, 5H, arom); 7.28 (t J = 7.50 Hz, 1H, arom); 7.45 (t J = 7.85 Hz, 1H, arom); 7.84 (s, 1H, CH methylidene); 13.48 (br s, 1H, COOH). ^{13}C NMR (DMSO-$d_{6\delta}$): δ 30.8, 32.0, 45.6, 67.6 (CH_2); 116.7, 118.4, 122.7, 123.2, 126.4, 128.8, 129.1, 131.2, 134.5, 134.7, 141.9, 159.7 (C-5, CH methylidene, CH arom, Cq arom); 166.8 (C═O); 167.8 (COOH); 193.7 (C═S). Anal. ($C_{21}H_{19}NO_4S_2$) calcd: C 61.00; H 4.63; N 3.39; found: C 60.96; H 4.45; N 3.48.

4.1.2.5. 2-{(5Z)-4-oxo-5-[3-(3-phenoxypropoxyphenyl)methylidene]-2-thioxothiazolidin-3-yl}acetic acid ***6e.*** Yield 74%; yellow solid; m.p. 181–185 °C; ^{1}H NMR (DMSO-$d_{6\delta}$): δ 2.20 (m, 2H, CH_2); 4.14 (t J = 6.25 Hz, 2H, $CH_2OC_6H_5$); 4.21 (t J = 6.25 Hz, 2H, OCH_2); 4.74 (s, 2H, NCH_2); 6.92 (t J = 7.30 Hz, 1H, arom); 6.95 (m, 2H, arom); 7.13 (dd J = 8.30 Hz J = 2.20 Hz, 1H, arom); 7.20–7.29 (m, 4H, arom); 7.47 (t J = 8.0 Hz, 1H, arom); 7.86 (s, 1H, CH methylidene); 13.47 (br s, 1H, COOH). ^{13}C NMR (DMSO-$d_{6\delta}$): δ 29.1, 45.6, 64.6, 65.2 (CH_2); 115.0, 117.0, 118.4, 121.1, 122.8, 123.2, 130.1, 131.2, 134.4, 134.7, 159.0, 159.5 (C-5, CH methylidene, CH arom, Cq arom); 166.8 (C═O); 167.8 (COOH); 193.8 (C═S). Anal. ($C_{21}H_{19}NO_5S_2$) calcd: C 58.73; H 4.46; N 3.26; found: C 58.63; H 4.33; N 3.19.

4.1.2.6. 2-{(5Z)-4-oxo-5-[3-(4-phenylbutoxyphenyl)methylidene]-2-thioxothiazolidin-3-yl}acetic acid ***6f.*** Yield 90%; yellow solid; m.p. 157–160 °C; ^{1}H NMR (DMSO-$d_{6\delta}$): δ 1.73 (m, 4H, 2 CH_2); 2.64 (m, 2H, $CH_2C_6H_5$); 4.03 (m, 2H, OCH_2); 4.74 (s, 2H, NCH_2); 7.07 (d J = 8.10 Hz, 1H, arom); 7.15–7.21 (m, 4H, arom); 7.27 (t J = 7.45 Hz, 2H, arom); 7.45 (t J = 8.15 Hz, 1H, arom); 7.84 (s, 1H, CH methylidene); 13.48 (br s, 1H, COOH). ^{13}C NMR (DMSO-$d_{6\delta}$): δ 27.9, 28.7, 35.3, 45.6, 68.1 (CH_2); 116.9, 118.3, 122.7, 123.1, 126.1, 128.7, 129.0, 131.2, 134.5, 134.7, 142.5, 159.7 (C-5, CH methylidene, CH arom, Cq arom); 166.8 (C═O); 167.8 (COOH); 193.7 (C═S). Anal. ($C_{22}H_{21}NO_4S_2$) calcd: C 61.81; H 4.95; N 3.28; found: C 61.74; H 4.64; N 3.19.

4.1.3. General procedure for the synthesis of 3-(5-arylidene-4-oxo-2-thioxothiazolidin-3-yl)propanoic acids ***7a-f***

A mixture of 3-(4-oxo-2-thioxothiazolidin-3-yl)propanoic acid (0.43 g, 2.09 mmol),sodium acetate (2.13 g, 15.6 mmol) and the appropriate aldehyde **10** (2.09 mmol) in glacial acetic acid (10 mL), was refluxed for 4–5 h. The mixture was cooled and poured into H_2O, providing a precipitate which was filtered off, washed with H_2O and recrystallized from methanol to give pure 3-[(5-arylidene-4-oxo-2-thioxothiazolidin-3-yl)] propanoic acids **7a-f**.

4.1.3.1. 3-{(5Z)-4-oxo-5-[4-(3-phenylpropoxyphenyl)methylidene]-2-thioxothiazolidin-3-yl}propanoic acid ***7a.*** Yield 28%; yellow solid; m.p. 178–182 °C; ^{1}H NMR (DMSO-$d_{6\delta}$): δ 2.04 (m, 2H, CH_2); 2.63 (t J = 7.50 Hz, 2H, CH_2COOH); 2.75 (t J = 7.95 Hz, 2H, C$H_2C_6H_5$); 4.06 (t J = 6.30 Hz, 2H, OCH_2); 4.23 (t J = 7.90 Hz, 2H, NCH_2); 7.11 (m, 2H, arom); 7.18 (m, 1H, arom); 7.22–7.24 (m, 2H, arom); 7.27–7.30 (m, 2H, arom); 7.60 (m, 2H, arom); 7.77 (s, 1H, CH methylidene); 12.50 (br s, 1H, COOH). ^{13}C NMR (DMSO-$d_{6\delta}$): δ 30.8, 31.4, 31.9, 40.5, 67.8 (CH_2); 116.2, 119.5, 126.0, 126.4, 128.9, 129.0, 133.6, 133.8, 141.8, 161.5 (C-5, CH methylidene, CH arom, Cq arom); 167.3 (C═O); 172.3(COOH); 193.7 (C═S). Anal. ($C_{22}H_{21}NO_4S_2$) calcd: C 61.81; H 4.95; N 3.28; found: C 61.55; H 4.84; N 3.22.

4.1.3.2. 3-{(5Z)-4-oxo-5-[4-(3-phenoxypropoxyphenyl)methylidene]-2-thioxothiazolidin-3-yl}propanoic acid ***7b.*** Yield 72%; yellow solid; m.p. 146–148 °C; ^{1}H NMR (DMSO-$d_{6\delta}$): δ 2.19 (m, 2H, CH_2); 2.62 (t J = 7.65 Hz, 2H, CH_2COOH); 4.12 (t J = 6.20 Hz, 2H, NCH_2); 4.20–4.23 (m, 4H, 2 OCH_2); 6.92 (t J = 7.35 Hz, 1H, arom); 6.94 (d J = 8.50 Hz, 2H, arom); 7.12 (m, 2H, arom); 7.27 (t J = 7.50 Hz, 2H, arom); 7.57 (m, 2H, arom); 7.74 (s, 1H, CH methylidene); 12.54 (br s, 1H, COOH). ^{13}C NMR (DMSO-$d_{6\delta}$): δ 29.1, 31.4, 40.6, 64.5, 64.7 (CH_2); 115.0, 116.2, 119.6, 121.1, 126.1, 130.1, 133.5, 133.8, 159.0, 161.4 (C-5, CH methylidene, CH arom, Cq arom); 167.3 (C═O); 172.3 (COOH); 193.6 (C═S). Anal. ($C_{22}H_{21}NO_5S_2$) calcd: C 59.98; H 4.77; N 3.16; found: C 60.11; H 4.65; N 3.08.

4.1.3.3. 3-{(5Z)-4-oxo-5-[4-(4-phenylbutoxyphenyl)methylidene]-2-thioxothiazolidin-3-yl}propanoic acid ***7c.*** Yield 40%; yellow solid; m.p. 152–155 °C; ^{1}H NMR (DMSO-$d_{6\delta}$): δ 1.73 (m, 4H, 2 CH_2); 2.63 (m, 4H, $CH_2C_6H_5$ + CH_2COOH); 4.08 (t J = 5.95 Hz, 2H, OCH_2); 4.23 (t J = 7.90, 2H, NCH_2); 7.10 (m, 2H, arom); 7.17 (m, 1H, arom); 7.21 (m, 2H, arom); 7.28 (m, 2H, arom), 7.59 (m, 2H, arom); 7.77 (s, 1H, CH methylidene); 12.46 (br s, 1H, COOH). ^{13}C NMR (DMSO-$d_{6\delta}$): δ 27.9, 28.6, 31.4, 35.3, 40.5, 68.3 (CH_2); 116.1, 119.5, 125.9, 128.7, 129.0, 133.4, 133.7, 133.9, 142.5, 161.6 (C-5, CH methylidene, CH arom, Cq arom); 167.3 (C═O); 172.3 (COOH); 193.6 (C═S). Anal. ($C_{23}H_{23}NO_4S_2$) calcd: C 62.56; H 5.25; N 3.17; found: C 62.38; H 5.10; N 3.22.

4.1.3.4. 3-{(5Z)-4-oxo-5-[3-(3-phenylpropoxyphenyl)methylidene]-2-thioxothiazolidin-3-yl}propanoic acid ***7d.*** Yield 57%; yellow solid; m.p. 138–141 °C; ^{1}H NMR (DMSO-$d_{6\delta}$): δ 2.04 (m, 2H, CH_2); 2.64 (t J = 7.70 Hz, 2H, CH_2COOH); 2.75 (t J = 7.70 Hz, 2H, $CH_2C_6H_5$); 4.01 (t J = 6.40 Hz, 2H, OCH_2); 4.23 (t J = 7.80 Hz, 2H, NCH_2); 7.07 (d J = 8.30 Hz, 1H, arom); 7.15–7.24 (m, 3H, arom); 7.28 (t J = 7.55 Hz, 1H, arom); 7.44 (t J = 7.90 Hz, 1H, arom); 7.76 (s, 1H, CH methylidene); 12.52 (br s, 1H, COOH). ^{13}C NMR (DMSO-$d_{6\delta}$): δ 30.8, 31.3, 32.0, 40.6, 67.6 (CH_2); 116.6, 118.1, 123.0, 123.2, 128.9, 131.2, 133.5, 134.8, 141.9, 159.6 (C-

5, CH methylidene, CH arom, Cq arom); 167.2 (C═O); 172.3 (COOH); 193.8 (C═S). Anal. ($C_{22}H_{21}NO_4S_2$) calcd: C 61.81; H 4.95; N 3.28; found: C 61.45; H 4.79; N 3.12.

4.1.3.5. 3-{(5Z)-4-oxo-5-[3-(3-phenoxypropoxyphenyl)methylidene]-2-thioxothiazolidin-3-yl}propanoic acid ***7e****.* Yield 76%; yellow solid; m.p. 140–141 °C; ^{1}H NMR (DMSO-d_6): δ 2.19 (m, 2H, CH_2); 2.63 (t J = 7.65 Hz, 2H, CH_2COOH); 4.13 (t J = 6.05 Hz, 2H, NCH_2); 4.18–4.24 (m, 4H, 2 OCH_2); 6.90–6.95 (m, 3H, arom); 7.09 (d J = 7.95 Hz, 1H, arom); 7.15–7.18 (m, 2H, arom); 7.27 (m, 2H, arom); 7.44 (t J = 7.85 Hz, 1H, arom); 7.75 (s, 1H, CH methylidene); 12.53 (br s, 1H, COOH). ^{13}C NMR (DMSO-d_6): δ 29.2, 31.3, 40.6, 64.6, 65.1 (CH_2); 115.0, 116.8, 118.1, 121.1, 123.0, 123.3, 130.0, 131.2, 133.4, 134.9, 159.0, 159.5 (C-5, CH methylidene, CH arom, Cq arom); 167.1 (C═O); 172.3 (COOH); 193.7 (C═S). Anal. ($C_{22}H_{21}NO_5S_2$) calcd: C 59.58; H 4.77; N 3.16; found: C 59.45; H 4.45; N 3.10.

4.1.3.6. 3-{(5Z)-4-oxo-5-[3-(4-phenylbutoxyphenyl)methylidene]-2-thioxothiazolidin-3-yl}propanoic acid ***7f****.* Yield 45%; yellow solid; m.p. 118–120 °C; ^{1}H NMR (DMSO-d_6): δ 1.74 (m, 4H, 2 CH_2); 2.64 (m, 4H, 2 CH_2); 4.04 (m, 2H, OCH_2); 4.23 (t J = 7.90 Hz, 2H, NCH_2); 7.07 (d J = 8.4 Hz, 1H, arom); 7.17 (m, 3H, arom); 7.21–7.22 (m, 2H, arom); 7.26–7.29 (m, 2H, arom); 7.44 (t J = 8.20 Hz, 1H, arom); 7.77 (s, 1H, CH methylidene); 12.51 (br s, 1H, COOH). ^{13}C NMR (DMSO-d_6): δ 27.9, 28.7, 31.3, 35.3, 40.6, 68.1 (CH_2); 116.8, 118.1, 123.0, 123.2, 126.4, 128.7, 129.0, 131.2, 133.5, 134.8, 142.5, 159.7 (C-5, CH methylidene, CH arom, Cq arom); 167.2 (C═O); 172.3 (COOH); 193.8 (C═S). Anal. ($C_{23}H_{23}NO_4S_2$) calcd: C 62.56; H 5.25; N 3.17; found: C 62.49; H 4.99; N 3.02.

4.2. Molecular docking

X-ray crystal structure selection and preparation of the AKR1B1-idose complex (PDB-ID: 3V36) [40] and PTP1B (PDB-ID: 1Q6T) [41] were performed as described in our previous studies [31,32]. Docking studies with GOLD (version 2020) [42] were performed into the catalytic site of PTP1B and AKR1B1, into the AKR1B1-idose complex and into the previously described allosteric binding pocket of PTP1B [31,32]. 25 Docking poses were generated with standard settings using the scoring function CHEMPLP. The obtained binding modes were subsequentially clustered based on LigandScouts [43,44] pharmacophore RDF-Code (radial distribution function) similarity. The docking poses were minimized in LigandScout with the MMFF94 force field [45]. 3D Pharmacophores were developed using LigandScout and 3D depictions of protein-ligand complexes were rendered in MOE (version 2020) [46].

4.3. Enzymatic assays

4.3.1. Expression and purification of human recombinant AKRB1, PTP1B and TC-PTP

The human recombinant AKR1B1 was expressed in BL21(DE3)pLysS *E. coli* cells and purified to electrophoretic homogeneity as previously described [47].

The sequences of both human PTP1B (1–303 aa, Uniprot code P18031) and human TC-PTP (1–415 aa, Uniprot code: P17706-1) coding sequences were cloned into bacterial expression vector (pNic28-Bsa4) downstream and in frame with polyHis tag following the procedure described by Luti et al. [48]. The bacterial vectors containg the sequences of human proteins were then used to tranform BL21(DE3) pLysS *E. coli* strain. Bacteria were grown in LB broth and, once they reached 0.8 OD, they were incubated overnight at 18 °C with 0.04 mM IPTG to induce fusion proteins synthesis. After expression, bacteria were lysed and recombinant proteins separated by bacterial proteins using a chromatographic column loaded with Ni-NTA Resin (Thermo Fischer Thermo Fisher Scientific 168 Third Avenue Waltham, MA USA). After elution, fractions containing PTP1B and TC-PTP were collected, concentrated and purified using a AKTA pure system equipped with a Superdex G75 column equilibrated with Tris-HCl buffer pH 8.0 containing 150 mM NaCl and 1 mM mercaptoethanol. The fractions containing PTP1B and TC-PTP were collected and analysed using SDS-PAGE to evaluate the protein purity degree. The solutions containing purified enzymes were split into fraction of 0.5 mL volume and each fraction stored at −80 °C.

4.3.2. Enzymatic assays

The purified AKR1B1 (specific activity 5.0 U/mg), stored at −80 °C in 10 mM sodium phosphate buffer pH 7.0 containing 2 mM dithiothreitol and 30% (w/v) glycerol, was extensively dialyzed against 10 mM sodium phosphate buffer pH 7.0 before use. AKR1B1 activity was determined at 37 °C as previously described [49] by evaluating the decrease in absorbance at 340 nm linked to NADPH oxidation (exctintion coefficient 6.22 mM^{-1} cm^{-1}). The standard assay mixture (0.7 mL finale volume) contained 0.25 M sodium phosphate buffer pH 6.8, 0.18 mM NADPH, 0.4 M ammonium sulfate, 0.5 mM EDTA and 4.7 mM GAL. The reaction was started by addition of the substrate. The NADPH oxidation rate measured in the absence of substrate was subtracted as blank. One unit of enzyme activity is the amount that catalyzes the conversion of 1 μmol of substrate/min in the above assay conditions.

The activity of PTP1B and TC-PTP was determined as previously described [50].

4.3.3. Inhibition studies on AKR1B1, PTP1B and TC-PTP

The determination of IC_{50} (concentration of compound required to determine 50% inhibition of enzyme activity) values was performed in the above described assay conditions, by using 2 mM L-idose as substrate. All compounds tested as AKR1B1 inhibitors were dissolved in DMSO and added to the assay mixture containing 8 mU of purified AKR1B1 (67 nM final concentration in the assay mixture, calculated on the basis of AKR1B1 molecular weight of 34 Kda).

The reaction was started by addition of the substrate. The DMSO concentration in all the assays was kept constant at 0.5% (v/v) in order to avoid effects on AKR1B1 activity [51].

PTP1B activity was determined as follows. An aliquot of human recombinant PTP1B was diluted in the assay buffer containing 0.075 M β,β-dimethylglutarate pH 7.0, 1 mM EDTA, 0.1 mM DTT and *p*-nitrophenyl phosphate (pNPP) as substrate. After an appropriate interval time, the reaction was stopped by diluting the assay solution with 2 mL of KOH 0.1 M.

The amount of *p*-nitrophenol (pNP) released was determined measuring the absorbance of the solution at 400 nm using a spectrophotometer and a 1-cm optical pathlength (εmM of pNP is 18).

The IC_{50} value for PTP1B was determined by measuring the pNPP hydrolysis rate in the presence of increasing inhibitor concentration. For each inhibitor, 15–16 different concentrations were used. All tests were carried out in triplicate and obtained data were normalized to control sample.

The IC_{50} values were determined by nonlinear regression analysis by using Prism GraphPad 7.04 fitting experimental data to the following equation:

$$\frac{v_i}{v_0} = \frac{Max - Min}{1 + \left(\frac{I}{IC_{50}}\right)^{slope}} + Min \qquad \text{(Equation 1)}$$

In equation (1), v_i/v_0, represents the ratio between the activity measured in the presence of the inhibitor and the activity measured in the absence of inhibitor; Max and Min represent the expected maximal and minimal value of the activity ratio and were fixed at 1 and zero, respectively. Slope, which describes the steepness of curve in the transition region, was fixed at −1. For each compound, at least five different concentrations of inhibitor, each tested at least in triplicate, were analysed.

4.3.4. Evaluation of action mechanism of inhibitors

The kinetic analysis was performed by measuring reaction rates with different L-idose concentrations in the absence and in the presence of different inhibitor concentrations. Data were analysed by Linewever-Burk plots. The inhibition constants K_i (apparent dissociation constant of the EI complex) and K_i' (apparent dissociation constant of the ESI complex) were determined from secondary plots of $1/V_{max}$ and K_M/V_{max} as a function of the inhibitor concentration, respectively. In the case of tight binding inhibitors (i.e. IC_{50} values of the same order of magnitude of enzyme concentration), the residual activity measurements obtained at each substrate concentration were fitted by nonlinear regression analysis to Morrison equation [52]:

$$v_i = 1 - \frac{([E_T] + [I] + K_i^{app}) - \sqrt{([E_T] + [I] + K_i^{app})^2 - 4[E_T][I]}}{2[E_T]}$$

for K_i^{app} evaluation. In order to obtain the inhibition constants K_i and K_i', the K_i^{app} values were plotted against substrate concentration, and fitted by nonlinear regression analysis to the equation:

$$K_i^{app} = ([S] + K_M) \,/\, (K_M \,/\, K_i + [S] \,/\, K_i') \qquad \text{(Equation 2)}$$

relative to a general case of tight binding non-competitive inhibition model. The used K_M value for L-idose, was 3.8 mM [47].

In order to evaluate the reversibility of the inhibitory action, 8 mU of purified AKR1B1were assayed in the presence of an inhibitor concentration able to reduce AKR1B1 activity to at least 75% of the control value. The mixture was then extensively dialysed on Amicon ultrafiltration membrane (cut off 10 KDa) against 10 mM sodium phosphate buffer, pH 7.0. After dialysis, the enzyme activity was again measured as above and compared to that of a mixture in the absence of inhibitor and treated in the same conditions.

As concerns PTP1B, detailed kinetic analyses were carried out to dissect action mechanism of compounds **6c, 6f, 7c** and **7f**.

The reversibility of inhibitory activity of compounds, was evaluated by dilution assay. An aliquot of the enzyme was incubated for 60 min at 37 °C in the presence of saturating amount of PTP1B inhibitor. After this time, an aliquot of the enzyme was withdrawn and diluted 400 folds in the assay buffer containing 2.5 mM of pNPP. After 15 min, the reaction was stopped by adding 1 mL of KOH 0.2 M. The amount of pNP released was calculated by measuring the absorbance at 400 nm of solutions using a spectrophotometer.

Data obtained were normalized to control tests, which were carried out by diluting the enzyme with DMSO, the solvent used to dissolve all compounds. Data reported in figure represent the mean value±S.E.M. (n = 3).

The impact of inhibitors on the main kinetic parameters, K_M and V_{max}, was calculated measuring the initial hydrolysis rate of PTP1B in the presence of increasing pNPP concentration (seven different concentrations in the 0.5–25 mM range) and different concentration of each inhibitor. All assays were carried out in triplicate. Data obtained were fitted using the Michaelis-Menten equation. To evaluate the action mechanism of inhibitors, the dependence of K_M and V_{max} from inhibitor concentration was studied, by using at least three different inhibitor concentrations. Data obtained were then analysed by double reciprocal plot (Lineweaver-Burk plot).

4.4. Ex Vivo assays

4.4.1. Cell cultures

Murine myoblasts (C2C12) were purchased by SigmaAldrich, which obtained them from the European Collection of Authenticated Cell Cultures (ECACC). C2C12 cells were grown in Dulbecco's Modified Eagle's medium (DMEM) supplemented with 10% foetal bovine serum (FBS), 2 mM glutamine, 100 IU/mL penicillin, 100 μg/mL streptomycin (Sigma-Aldrich, St. Louis, MO, USA), in a humidified atmosphere and with 5% CO_2 at 37 °C. Differentiation of C2C12 was induced incubating murine myoblasts in DMEM supplemented with 2% horse serum. C2C12 cells were plated and grown until they reach 70% confluence. Then, cells were incubated in the presence of 2% horse serum for 96 h. Every 48 h, the medium was replaced with fresh medium. After 96 h, the degree of differentiation was evaluated by analysing cells with a contrast phase microscope.

The human lens epithelial line B3 (HLE) cells were obtained from American Type Culture Collection (Rockville, MD, USA) and cultured at 37 °C in Eagle's modified essential medium (MEM) supplemented with 20% (v/v) FBS, 50 mU/mLpenicillin/streptomycin and 2 mM glutamine (complete medium) in a humidified atmosphere with 5% CO_2.

4.4.2. Cell viability assays

C2C12 cells were incubated in the presence of increasing concentrations of compounds **6c, 6f, 7c** and **7f** for 48 h at 37 °C. After this time, cells were washed with PBS and then incubated for 1 h with 0.5 mg/mL of MTT dissolved in complete medium. Then cells were washed and lysed with 300 μL of DMSO. The absorbance of solutions were evaluated using a microplate readers at 595 nm. All data were normalized respect to control experiment. Data showed in the figure represent the mean values ± S.E.M. (n = 4).

HLE cells were incubated at 37 °C in complete medium in the presence of the indicated inhibitor concentration for 24 and 48 h. Then cells were washed with PBS and incubated for 1 h with 0.5 mg/mL of MTT dissolved in a phosphate buffer solution pH 7.4. The formazane crystals were then dissolved by the addition of 0.04 N HCl in isopropanol, and the absorbance of the solution at 563 nm was measured using a microplate reader.

4.4.3. Evaluation of insulin-mimetic/sensibilizing activity of PTP1B inhibitors

Differentiated C2C12 cells were starved for 24 h and then incubated in the presence of compounds **6c, 6f, 7c** and **7f** (20 μM, final concentration) for 90 min. After this time, cells were washed with PBS and then stimulated or not with 10 nM insulin for 30 min. Then, cells were lysed and cellular proteins separated on a 12% SDS-PAGE. After electrophoresis, cellular proteins were transferred on a PVDF membrane by Western blot technique and then probed against antibodies able to specifically recognize IR (I2033 Sigma Aldrich) or phosphorylated form of IR (MABS65, Sigma-Aldrich). Sample loading was evaluated probing PVDF membrane with anti-actin antibodies (ABT1485 Sigma Aldrich).

4.4.4. Glucose uptake assay

C2C12 cells sedeed in 24 multiwell plates were serum-starved for 24 h and then stimulated with 10 nM insulin, with 20 μM of compounds **6f** and **7f** of with combination (insulin + compounds) for 15 min. After this time, starvation medium was removed, cells washed with PBS and then incubated with starvation medium containing 40 μM of 2-NBDG. After 3 h, medium was removed, and cells detached using trypsin. Collected cells were washed with PBS and then analysed using a FACS Canto II flow cytometer (BD Bioscence). All tests were carried out in quadruplicate.

4.4.5. Determination of sorbitol content

After exposure to hyperglycemic conditions, HLE cells were washed with PBS supplemented with 1 mM PMSF, harvested and lysed by means of three freezing/thawing cycles. The supernatant obtained after centrifugation at 10,000×*g* at 4 °C per 30 min (crude HLE cells extract) was supplemented with 4 M ice cold perchloric acid. Samples were then neutralized using 5 M KOH and the sorbitol content measured as described [53]. Protein content was measured on the crude HLE cells extract according to Bradford [54].

Funding

This research did not receive any specific grant from funding agencies in the public, commercial or not-for-profit sectors.

Declaration of competing interest

The authors declare that they have no known competing financial interests or personal relationships that could have appeared to influence the work reported in this paper.

Data availability

No data was used for the research described in the article.

Appendix A. Supplementary data

Supplementary data to this article can be found online at https://doi.org/10.1016/j.ejmech.2023.115270.

References

[1] H. Sun, P. Saeedi, S. Karuranga, M. Pinkepank, K. Ogurtsova, B.B. Duncan, C. Stein, A. Basit, J.C.N. Chan, J.C. Mbanya, M.E. Pavkov, A. Ramachandaran, S.H. Wild, S. James, W.H. Herman, P. Zhang, C. Bommer, S. Kuo, E.J. Boyko, D.J. Magliano, IDF Diabetes atlas: global, regional and country-level diabetes prevalence estimates for 2021 and projections for 2045, Diabetes Res. Clin. Pract. 183 (2022) 109119–109132, https://doi.org/10.1016/j.diabres.2021.109119.

[2] R. Viner, B. White, D. Christie, Type 2 diabetes in adolescents: a severe phenotype posing major clinical challenges and public health burden, Lancet 389 (2017) 2252–2260, https://doi.org/10.1016/S0140-6736(17)31371-5.

[3] R. Morphy, Z. Rankovic, Designed multiple ligands. An emerging drug discovery paradigm, J. Med. Chem. 48 (2005) 6523–6543, https://doi.org/10.1021/jm058225d.

[4] P. Csermely, V. Agoston, S. Pongor, The efficiency of multi-target drugs: the network approach might help drug design, Trends Pharmacol. Sci. 26 (2005) 178–182, https://doi.org/10.1016/j.tips.2005.02.007.

[5] E. Proschak, H. Stark, D. Merk, Polypharmacology by design: a medicinal chemist's perspective on multitargeting compounds, J. Med. Chem. 62 (2019) 420–444, https://doi.org/10.1021/acs.jmedchem.8b00760.

[6] M. Elchebly, P. Payette, E. Michaliszyn, W. Cromlish, S. Collins, A.L. Loy, D. Normandin, A. Cheng, J. Himms-Hagen, C. Chan, C. Ramachandran, M. J. Gresser, M.L. Tremblay, B.P. Kennedy, Increased insulin sensitivity and obesity resistance in mice lacking the protein tyrosine phosphatase-1B gene, Science 283 (1999) 1544–1548, https://doi.org/10.1126/science.283.5407.1544.

[7] Z.Y. Zhang, G.T. Dodd, T. Tiganis, Protein tyrosine phosphatases in hypothalamic insulin and leptin signaling, Trends Pharmacol. Sci. 36 (2015) 661–674, https://doi.org/10.1016/j.tips.2015.07.003.

[8] S. Koren, I.G. Fantus, Inhibition of the protein tyrosine phosphatase PTP1B: potential therapy for obesity, insulin resistance and type-2 diabetes mellitus, Best Pract. Res. Clin. Endocrinol. Metabol. 21 (2007) 621–640, https://doi.org/10.1016/j.beem.2007.08.004.

[9] A.P. Combs, Recent advances in the discovery of competitive protein tyrosine phosphatase 1B inhibitors for the treatment of diabetes, obesity and cancer, J. Med. Chem. 53 (2010) 2333–2344, https://doi.org/10.1021/jm901090b.

[10] K.A. Lantz, S.G.E. Hart, S.L. Planey, M.F. Roitman, I.A. Ruiz-White, H.R. Wolfe, M. P. McLane, Inhibition of PTP1B by trodusquemine (MSI-1436) causes fat-specific weight loss in diet-induced obese mice, Obesity 18 (2010) 1516–1523, https://doi.org/10.1038/oby.2009.444.

[11] L.J. Wang, B. Jiang, N. Wu, S.Y. Wang, D.Y. Shi, Natural and semisynthetic protein tyrosine phosphatase 1B (PTP1B) inhibitors as anti-diabetic agents, RSC Adv. 5 (2015) 48822–48834, https://doi.org/10.1039/C5RA01754H.

[12] S. Thakur, S.K. Gupta, V. Ali, P. Singh, M. Verma, Aldose reductase: a cause and a potential target for the treatment of diabetic complications, Arch Pharm. Res. (Seoul) 44 (2021) 655–667, https://doi.org/10.1007/s12272-021-01343-5.

[13] R. Maccari, R. Ottanà, Targeting aldose reductase for the treatment of diabetes complications and inflammatory diseases: new insights and future directions, J. Med. Chem. 58 (2015) 2047–2067, https://doi.org/10.1021/jm500907a.

[14] N. Hotta, Y. Akanuma, R. Kawamori, K. Matsuoka, Y. Oka, M. Shichiri, T. Toyota, M. Nakashima, I. Yoshimura, N. Sakamoto, Y. Shigeta, Long-term clinical effects of epalrestat, an aldose reductase inhibitor, on diabetic peripheral neuropathy, Diabetes Care 29 (2006) 1538–1544, https://doi.org/10.1111/j.1464-5491.2012.03684.x.

[15] K.V. Ramana, S.K. Srivastava, Aldose reductase: a novel therapeutic target for inflammatory pathologies, Int. J. Biochem. Cell Biol. 42 (2010) 17–20, https://doi.org/10.1016/j.biocel.2009.09.009.

[16] M. Hlavac, L. Kovacikova, M.S. Prnova, G. Addova, G. Hanquet, M. Stefek, A. Bohac, Novel substituted N-benzyl(oxotriazinoindole) inhibitors of aldose reductase exploiting ALR2 unoccupied interactive pocket, Bioorg. Med. Chem. 29 (2021), 115885, https://doi.org/10.1016/j.bmc.2020.115885.

[17] G. Bruno, L. Costantino, C. Curinga, R. Maccari, F. Monforte, F. Nicolò, R. Ottanà, M.G. Vigorita, Synthesis and aldose reductase inhibitory activity of 5-arylidene-2,4-thiazolidinediones, Bioorg. Med. Chem. 10 (2002) 1077–1084, https://doi.org/10.1016/S0968-0896(01)00366-2.

[18] R. Maccari, R. Ottanà, C. Curinga, M.G. Vigorita, D. Rakowitz, T. Steindl, T. Langer, Structure–activity relationships and molecular modelling of 5-arylidene-2,4-thiazolidinediones active as aldose reductase inhibitors, Bioorg. Med. Chem. 13 (2005) 2809–2823, https://doi.org/10.1016/j.bmc.2005.02.026.

[19] R. Maccari, R. Ottanà, R. Ciurleo, M.G. Vigorita, D. Rakowitz, T. Steindl, T. Langer, Evaluation of *in vitro* aldose reductase inhibitory activity of 5-arylidene-2,4-thiazolidinediones, Bioorg. Med. Chem. Lett. 17 (2007) 3886–3893, https://doi.org/10.1016/j.bmcl.2007.04.109.

[20] R. Maccari, R. Ottanà, R. Ciurleo, D. Rakowitz, B. Matuszczak, C. Laggner, T. Langer, Synthesis, induced-fit docking investigations, and *in vitro* aldose reductase inhibitory activity of non-carboxylic acid containing 2,4-thiazolidine-dione derivatives, Bioorg. Med. Chem. 16 (2008) 5840–5852, https://doi.org/10.1016/j.bmc.2008.04.072.

[21] R. Maccari, R. Ciurleo, M. Giglio, M. Cappiello, R. Moschini, A. Del Corso, U. Mura, R. Ottanà, Identification of new non-carboxylic acid containing inhibitors of aldose reductase, Bioorg. Med. Chem. 18 (2010) 4049–4055, https://doi.org/10.1016/j.bmc.2010.04.016.

[22] R. Ottanà, R. Maccari, M. Giglio, A. Del Corso, M. Cappiello, U. Mura, S. Cosconati, L. Marinelli, E. Novellino, S. Sartini, C. La Motta, F. Da Settimo, Identification of 5-arylidene-4-thiazolidinone derivatives endowed with dual activity as aldose reductase inhibitors and antioxidant agents for the treatment of diabetic complications, Eur. J. Med. Chem. 46 (2011) 2797–2806, https://doi.org/10.1016/j.ejmech.2011.03.068.

[23] R. Maccari, A. Del Corso, M. Giglio, R. Moschini, U. Mura, R. Ottanà, *In vitro* evaluation of 5-arylidene-2-thioxo-4-thiazolidinones active as aldose reductase inhibitors, Bioorg. Med. Chem. Lett. 21 (2011) 200–203, https://doi.org/10.1016/j.bmcl.2010.11.041.

[24] R. Maccari, R.M. Vitale, R. Ottanà, M. Rocchiccioli, A. Marrazzo, V. Cardile, A.C. E. Graziano, P. Amodeo, U. Mura, A. Del Corso, Structure-activity relationships and molecular modelling of new 5-arylidene-4-thiazolidinone derivatives as aldose reductase inhibitors and potential anti-inflammatory agents, Eur. J. Med. Chem. 81 (2014) 1–14, https://doi.org/10.1016/j.ejmech.2014.05.003.

[25] R. Maccari, P. Paoli, R. Ottanà, M. Jacomelli, R. Ciurleo, G. Manao, T. Steindl, T. Langer, M.G. Vigorita, G. Camici, 5-Arylidene-2,4-thiazolidinediones as inhibitors of protein tyrosine phosphatases, Bioorg. Med. Chem. 15 (2007) 5137–5149, https://doi.org/10.1016/j.bmc.2007.05.027.

[26] R. Ottanà, R. Maccari, R. Ciurleo, P. Paoli, M. Jacomelli, G. Manao, G. Camici, C. Laggner, T. Langer, 5-Arylidene-2-phenylimino-4-thiazolidinones as PTP1B and LMW-PTP inhibitors, Bioorg. Med. Chem. 17 (2009) 1928–1937, https://doi.org/10.1016/j.bmc.2009.01.044.

[27] R. Maccari, R. Ottanà, R. Ciurleo, P. Paoli, G. Manao, G. Camici, C. Laggner, T. Langer, Structure-based optimization of benzoic acids as inhibitors of protein tyrosine phosphatase 1B and low molecular weight protein tyrosine phosphatase, ChemMedChem 4 (2009) 957–962, https://doi.org/10.1002/cmdc.200800427.

[28] R. Ottanà, R. Maccari, S. Amuso, G. Wolber, D. Schuster, S. Herdlinger, G. Manao, G. Camici, P. Paoli, New 4-[(5-arylidene-2-arylimino-4-oxo-3-thiazolidinyl) methyl]benzoic acids active as protein tyrosine phosphatase inhibitors endowed with insulinomimetic effect on mouse C2C12 skeletal muscle cells, Eur. J. Med. Chem. 50 (2012) 332–343, https://doi.org/10.1016/j.ejmech.2012.02.012.

[29] R. Ottanà, R. Maccari, J. Mortier, A. Caselli, S. Amuso, G. Camici, A. Rotondo, G. Wolber, P. Paoli, Synthesis, biological activity and structure-activity relationships of new benzoic acid-based protein tyrosine phosphatase inhibitors endowed with insulinomimetic effects in mouse C2C12 skeletal muscle cells, Eur. J. Med. Chem. 71 (2014) 112–127, https://doi.org/10.1016/j.ejmech.2013.11.001.

[30] R. Ottanà, P. Paoli, A. Naß, G. Lori, V. Cardile, I. Adornato, A. Rotondo, A.C. E. Graziano, G. Wolber, R. Maccari, Discovery of 4-[(5-arylidene-4-oxothiazolidin-3-yl)methyl]benzoic acid derivatives active as novel potent allosteric inhibitors of protein tyrosine phosphatase 1B: in silico studies and *newly* evaluation as insulinomimetic and anti-inflammatory agents, Eur. J. Med. Chem. 127 (2017) 840–858, https://doi.org/10.1016/j.ejmech.2016.10.063.

[31] R. Maccari, A. Del Corso, P. Paoli, I. Adornato, G. Lori, F. Balestri, M. Cappiello, A. Naß, G. Wolber, R. Ottanà, An investigation on 4-thiazolidinone derivatives as dual inhibitors of aldose reductase and protein tyrosine phosphatase 1B, in the search for potential agents for the treatment of type 2 diabetes mellitus and its complications, Bioorg. Med. Chem. Lett. 28 (2018) 3712–3720, https://doi.org/10.1016/j.bmcl.2018.10.024.

[32] R. Ottanà, P. Paoli, M. Cappiello, T.N. Nguyen, I. Adornato, A. Del Corso, M. Genovese, I. Nesi, R. Moschini, A. Naß, G. Wolber, R. Maccari, In search for multi-target ligands as potential agents for diabetes mellitus and its complications-a structure-activity relationship study on inhibitors of aldose reductase and protein tyrosine phosphatase 1B, Molecules 26 (2021) 330, https://doi.org/10.3390/molecules26020330.

[33] R. Ottanà, R. Maccari, M.L. Barreca, G. Bruno, A. Rotondo, A. Rossi, G. Chiricosta, R. Di Paola, L. Sautebin, S. Cuzzocrea, M.G. Vigorita, 5-Arylidene-2-imino-4-thiazolidinones: design and synthesis of novel antiinflammatory agents, Bioorg. Med. Chem. 13 (2005) 4243–4252, https://doi.org/10.1016/j.bmc.2005.04.058.

[34] L.F. Iversen, K.B. Moller, A.K. Pedersen, G.H. Peters, A.S. Petersen, H.S. Andersen, S. Branner, S.B. Mortensen, N.P.H. Moller, Structure determination of T cell protein-tyrosine phosphatase, J. Biol. Chem. 277 (2002) 19982–19990, https://doi.org/10.1074/jbc.M200567200.

[35] G.R. Freidenberg, H.H. Klein, R. Cordera, J.M. Olefsky, Insulin receptor kinase activity in rat liver. Regulation by fasting and high carbohydrate feeding, J. Biol. Chem. 260 (1985) 12444–12453, https://doi.org/10.1016/S0021-9258(17)38893-2.

[36] C.L. Venable, E.U. Frevert, Y.B. Kim, B.M. Fischer, S. Kamatkar, B.G. Neel, B. B. Kahn, Overexpression of protein-tyrosine phosphatase-1B in adipocytes inhibits insulin-stimulated phosphoinositide 3-kinase activity without altering glucose transport or Akt/Protein kinase B activation, J. Biol. Chem. 275 (2000) 18318–18326, https://doi.org/10.1074/jbc.M908392199.

[37] J.E. Bleasdale, D. Ogg, B.J. Palazuk, C.S. Jacob, M.L. Swanson, X.Y. Wang, D. P. Thompson, R.A. Conradi, W.R. Mathews, A.L. Laborde, C.W. Stuchly, A. Heijbel, K. Bergdahl, C.A. Bannow, C.W. Smith, C. Svensson, C. Liljebris, H.J. Schostarez, P. D. May, F.C. Stevens, S.D. Larsen, Small molecule peptidomimetics containing a novel phosphotyrosine bioisostere inhibit protein tyrosine phosphatase 1B and augment insulin action, Biochemistry 40 (2001) 5642–5654, https://doi.org/10.1021/bi002865v.

[38] L. Xie, S.Y. Lee, J.N. Andersen, S. Waters, K. Shen, X.L. Guo, N.P. Moller, J. M. Olefsky, D.S. Lawrence, Z.Y. Zhang, Cellular effects of small molecule PTP1B inhibitors on insulin signaling, Biochemistry 42 (2003) 12792–12804, https://doi.org/10.1021/bi035238p.

[39] C. Wiesmann, K.J. Barr, J. Kung, J. Zhu, D.A. Erlanson, W. Shen, B.J. Fahr, M. Zhong, L. Taylor, M. Randal, R.S. McDowell, S.K. Hansen, Allosteric inhibition of protein tyrosine phosphatase 1B, Nat. Struct. Mol. Biol. 11 (2004) 730–737, https://doi.org/10.1038/nsmb803.

[40] X. Zheng, L. Zhang, W. Chen, Y. Chen, W. Xie, X. Hu, Partial inhibition of aldose reductase by nitazoxanide and its molecular basis, ChemMedChem 7 (2012) 1921–1923, https://doi.org/10.1002/cmdc.201200333.

[41] G. Scapin, S.B. Patel, J.W. Becker, Q. Wang, C. Desponts, D. Waddleton, K. Skorey, W. Cromlish, C. Bayly, M. Therien, J.Y. Gauthier, C.S. Li, C.K. Lau, C. Ramachandran, B.P. Kennedy, E. Asante-Appiah, The structural basis for the selectivity of benzotriazole inhibitors of PTP1B, Biochemistry 42 (2003) 11451–11459, https://doi.org/10.1021/bi035098j.

[42] G. Jones, P. Willett, R.C. Glen, A.R. Leach, R. Taylor, Development and validation of a genetic algorithm for flexible docking, J. Mol. Biol. 267 (1997) 727–748, https://doi.org/10.1006/jmbi.1996.0897.

[43] G. Wolber, T. Langer, LigandScout: 3-D pharmacophores derived from protein-bound ligands and their use as virtual screening filters, J. Chem. Inf. Model. 45 (2005) 160–169, https://doi.org/10.1021/ci049885e.

[44] G. Wolber, A.A. Dornhofer, T. Langer, Efficient overlay of small organic molecules using 3D pharmacophores, J. Comput. Mol. Des. 20 (2006) 773–788, https://doi.org/10.1007/s10822-006-9078-7.

[45] T.A. Halgren, Merck molecular force field. II. MMFF94 van der Waals and electrostatic parameters for intermolecular interactions, J. Comput. Chem. 17 (1996) 520–552, https://doi.org/10.1002/(SICI)1096-987X, 199604)17:5/6%3C520::AID-JCC2%3E3.0.CO;2-W.

[46] Molecular Operating Environment (MOE), 09 Chemical Computing Group ULC: Montreal, QC, Canada, 2020, p. 2022.

[47] F. Balestri, M. Cappiello, R. Moschini, R. Rotondo, I. Buggiani, P. Pelosi, U. Mura, A. Del Corso, L-Idose: an attractive substrate alternative to D-glucose for measuring aldose reductase activity, Biochem. Biophys. Res. Commun. 456 (2015) 891–895, https://doi.org/10.1016/j.bbrc.2014.12.054.

[48] S. Luti, S. Campigli, F. Ranaldi, P. Paoli, L. Pazzagli, G. Marchi, Lscβ and lscγ, two novel levansucrases of Pseudomonas syringae pv. actinidiae biovar 3, the causal agent of bacterial canker of kiwifruit, show different enzymatic properties, Int. J. Biol. Macromol. 179 (2021) 279–291, https://doi.org/10.1016/j.ijbiomac.2021.02.189.

[49] F. Balestri, M. Cappiello, R. Moschini, R. Rotondo, M. Abate, A. Del Corso, U. Mura, Modulation of aldose reductase activity by aldose hemiacetals, Biochim. Biophys. Acta 1850 (2015) 2329–2339, https://doi.org/10.1016/j.bbagen.2015.07.007.

[50] M. Genovese, C. Imperatore, M. Casertano, A. Aiello, F. Balestri, L. Piazza, M. Menna, A. Del Corso, P. Paoli, Dual targeting of PTP1B and aldose reductase with marine drug phosphoeleganin: a promising strategy for treatment of type 2 diabetes, Mar. Drugs 24 (2021) 535, https://doi.org/10.3390/md1910053.

[51] L. Misuri, M. Cappiello, F. Balestri, R. Moschini, V. Barracco, U. Mura, A. Del Corso, The use of dimethylsulfoxide as a solvent in enzyme inhibition studies: the case of aldose reductase, J. Enzym. Inhib. Med. Chem. 32 (2017) 1152–1158, https://doi.org/10.1080/14756366.2017.1363744.

[52] J.F. Morrison, Kinetics of the reversible inhibition of enzyme-catalysed reactions by tight-binding inhibitors, Biochim. Biophys. Acta 185 (1969) 269–286, https://doi.org/10.1016/0005-2744(69)90420-3.

[53] G.B. Reddy, A. Satyanarayana, N. Balakrishna, R. Ayyagari, M. Padma, K. Viswanath, J.M. Petrash, Erythrocyte aldose reductase activity and sorbitol levels in diabetic retinopathy, Mol. Vis. 14 (2008) 593–601. http://www.molvis.org/molvis/v14/a72.

[54] M.M. Bradford, A rapid and sensitive method for the quantitation of microgram quantities of protein utilizing the principle of protein-dye binding, Anal. Biochem. 72 (1976) 248–254, https://doi.org/10.1006/abio.1976.9999.